Realia et naturalia

DISSERTATIONES
PHYSICAE
UNIVERSITATIS
TARTUENSIS
83

KARL KRUUSAMÄE

Deformation-dependent electrode impedance of ionic electromechanically active polymers

DISSERTATIONES PHYSICAE UNIVERSITATIS TARTUENSIS
83

DISSERTATIONES PHYSICAE UNIVERSITATIS TARTUENSIS
83

KARL KRUUSAMÄE

Deformation-dependent electrode impedance of ionic electromechanically active polymers

UNIVERSITY OF TARTU
PRESS
1632

The study was carried out at the Institute of Physics, University of Tartu.

The Dissertation was admitted on October 19, 2012 in partial fulfillment of the requirements for the degree of Doctor of Philosophy in physics and allowed for defense by the Scientific Council of the Institute of Physics, University of Tartu.

Supervisors: Andres Punning, University of Tartu

Alvo Aabloo, University of Tartu

Opponents: Jonathan Rossiter, University of Bristol, United Kingdom

Mart Min, Tallinn University of Technology, Estonia

Defence: December 12, 2012 at University of Tartu, Tartu, Estonia

This research was funded in part by the Estonian Information Technology Foundation, European Social Fund's (ESF) Doctoral Studies and Internationalisation Programme DoRa carried out by Archimedes Foundation, and the graduate school "Functional materials and processes" receiving funding from the ESF under project 1.2.0401.09–0079 in Estonia.

ISSN 1406–0647
ISBN 978–9949–32–172–8 (print)
ISBN 978–9949–32–173–5 (pdf)

University of Tartu Press
www.tyk.ee
Order No 560

To my grandfather

TABLE OF CONTENTS

LIST OF ORIGINAL PUBLICATIONS

This thesis is based on the following papers referred to in the text by their Roman numerals. The papers are listed in the order of which they appear in the main article of this thesis. All papers are reprinted with kind permission from the publishers.

I. Karl Kruusamäe, Andres Punning, Alvo Aabloo (2012) **Electrical model of a carbon-polymer composite (CPC) collision detector**, Sensors, 12(2), 1950–1966.

II. Karl Kruusamäe, Paola Brunetto, Salvatore Graziani, Andres Punning, Giovanna Di Pasquale, Alvo Aabloo (2010) **Self-sensing ionic polymer-metal composite actuating device with patterned surface electrodes**, Polymer International, 59(3), 300–304.

III. Karl Kruusamäe, Paola Brunetto, Andres Punning, Margus Kodu, Raivo Jaaniso, Salvatore Graziani, Luigi Fortuna and Alvo Aabloo (2011) **Electromechanical model for a self-sensing ionic polymer-metal composite actuating device with patterned surface electrodes**, Smart Materials and Structures, 20(12), 124001.

Other papers relevant to this work but not included in this thesis.

- Indrek Must, Karl Kruusamäe, Urmas Johanson, Tarmo Tamm, Andres Punning, Alvo Aabloo (2012) **Characterisation of electromechanically active polymers using electrochemical impedance spectroscopy**, Lecture Notes on Impedance Spectroscopy: Measurement, Modeling and Applications 2, Olfa Kanoun (Ed.), CRC Press, 113–121.
- Karl Kruusamäe, Andres Punning, Alvo Aabloo (2011) **Self-sensing properties of carbon-polymer composite (CPC) actuators**, Proceedings of SPIE 7976, 79760Q.
- Karl Kruusamäe, Paola Brunetto, Salvatore Graziani, Luigi Fortuna, Margus Kodu, Raivo Jaaniso, Andres Punning, Alvo Aabloo (2010) **Experiments with self-sensing IPMC actuating device**, Proceedings of SPIE 7642, 76420V.
- Karl Kruusamäe, Andres Punning, Maarja Kruusmaa, Alvo Aabloo (2009) **Dynamical variation of the impedances of IPMC**, Proceedings of SPIE 7287, 72870V.

Author's contribution

Paper I: author conducted all the experimentation and data processing, and was responsible for writing the paper.

Paper II: author prepared the prototype, conducted all the experimentation, and was responsible for writing the paper.

Paper III: author was collaborating in preparing different samples, conducted all the analysis of created patterns, and was responsible for writing the paper.

LIST OF ABBREVIATIONS

(in alphabetical order)

CDC	carbide-derived carbon
cIEAP	IEAP with electrodes containing allotropes of carbon
CNC	computer numerical control
CNT	carbon nanotube
CPC	carbon-polymer composite
DAP	direct assembly process
DAQ	data acquisition
DC	direct current
DMAc	dimethylacetamide
EAP	electroactive polymer, electromechanically active polymer
EDLC	electrical double-layer capacitor
EIS	electrochemical impedance spectroscopy
$EMIMBF_4$	1-ethyl-3-methylimidazolium tetrafluoroborate
FTIR	Fourier transform infrared spectroscopy
IEAP	ionic EAP
IL	ionic liquid
IPMC	ionic polymer-metal composite
MALA	material-assisted laser ablation
MDOF	multi-degree-of-freedom
MEMS	microelectromechanical systems
mIEAP	IEAP with metal electrodes
NI	National Instruments
PC	personal computer
PCI	peripheral component interconnect
PTFE	polytetrafluoroethylene
PVC	poly(vinylchloride)
PVdF(HFP)	poly(vinylidene fluoride-co-hexafluoropropylene)
SWCNT	single-walled carbon nanotube

1. IONIC ELECTROMECHANICALLY ACTIVE POLYMERS

1.1. Introduction

Electromechanically active materials change their mechanical properties (e.g. shape) when electric stimulus is applied. Most typically the registered deformations are in the form of bending or stretching of a material. For that reason, a majority of these materials consist of elastic polymers, thus, proving the widely used acronym of EAP (electroactive polymers) for all such materials [1]. Furthermore, due to similarities to biological muscles, EAP materials are often referred to as artificial muscles.

Practically every EAP exhibits also mechanoelectrical sensor properties, *i.e.* by externally manipulating the actuators, alteration of voltage or some other type of electrical quantity can be registered [1–3].

The EAP materials can be divided into two principal classes:

1) Electronic EAP
2) Ionic EAP (IEAP)

Electronic EAPs (e.g. dielectric elastomers) exhibit alteration in their mechanical properties due to a variety of charging effects and/or Coulomb forces. However, in ionic EAPs the actuation is caused by dilatometric effects occurring due to electrically induced dislocation of mobile ions inside a polymer matrix.

There are many different application areas for EAP actuators ranging from designated micromachinery to home appliances. Out of the many advantages, the easy customisation, simple construction, and possibility to miniaturise are perhaps the most outstanding. For example, EAPs are often constructed in a trilayer configuration, where each layer can be customised to meet the requirements for a specific actuating device. Moreover, by simply cutting the EAP smaller, the actuation phenomenon remains, thus, allowing creation of rather miniature devices [4,5].

In applications, actuators often require means for closed-loop control and implementing the actuator itself as a feedback source on its behaviour is considered as self-sensing. While several types of EAP exhibit well-utilisable self-sensing properties [6,7], in the case of ionic polymer actuators there are several challenges.

The aim of this thesis is to advance the idea of self-sensing IEAP. For that purpose two distinctively different – metal- and carbon-based – trilayer IEAP actuators are studied from the perspective of structure and composition of electrodes. This thesis implements the electrochemical impedance spectroscopy in order to develop the electrical equivalent circuits of these two materials and describes relationship between the quantitative parameters and spatial shape of these IEAPs. Eventually prototypes of self-sensing systems of each type of material are designed, modelled and analysed.

Electronic EAP as well as ionic EAP with conducting polymer electrodes are not within the scope of this thesis.

The current chapter introduces the working mechanisms and key properties of several types of ionic EAP. In sections 1.2.–1.4. general principles of a variety of ionic EAPs are given.

1.2. IEAP actuators in brief

A typical IEAP consists of two conductive electrode layers separated by an electronically insulating but ion-permeable membrane. The composite structure also includes liquid electrolyte. For a flexible IEAP actuator in a cantilever configuration (*i.e.* one end of an actuator is fixed while the other end is able to move), when voltage in the range of a few volts is applied between the electrodes, a bending motion is registered (figure 1.1).

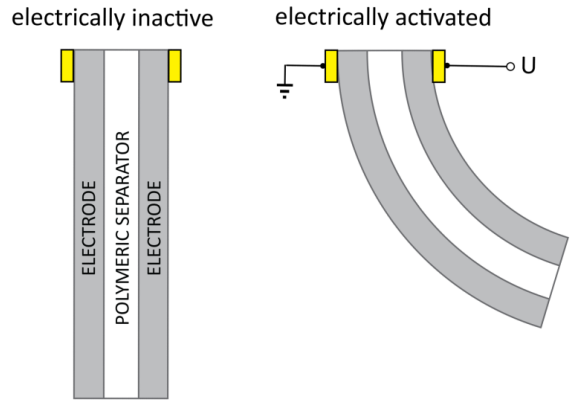

Figure 1.1. Behaviour of typical bending ionic EAP actuator.

In general, the actuation phenomenon is explained by the dislocation of ions due to electric field, thus, causing gradient in electrolyte concentration responsible for mechanical bending [1]. Therefore, it is necessary that the polymer backbone would either itself be ionic or penetrable for mobile ions. As an ionic polymer, Nafion and Flemion are the most commonly used [8], while examples of simply ion-permeable non-ionic materials include PVdF(HFP), PVC, paper, etc.

IEAPs can be categorised as wet and dry actuators depending on the environment they operate in. For stable and repeatable functioning, wet actuators need to be in a certain kind of solution such as deionised water or propylene carbonate. The role of this liquid solution can be different. In the case of water-containing IEAPs, the mobile ions become hydrated and therefore expansion of one electrode is due to an excess of both water molecules and ions. However,

the fast evaporation of water at room temperature causes a quick decrease in the performance of the actuator [9,10]. On the other hand, the liquid solution can carry the role of an electrolyte by containing mobile ions that migrate in and out of the IEAP actuator [11], thus, contributing to the performance of the actuator. Nevertheless, the so-called dry IEAP actuators can operate in diverse environments as the electrolyte contributing to actuation can be contained within the composite structure itself [12–14].

A relatively high specific area of an electrode material is of great importance in the design of an actuator. Besides the conductivity, a significant factor contributing to the actuation properties is capacitance between the electrodes of an IEAP sample characterising capability to accumulate electrical charge [15]. That means an IEAP is similar to an electrical double-layer capacitor (EDLC) where supercapacitive effect is achieved due to high specific area of electrode material. Each electrode is equivalent to a capacitor with capacitance (C_e) given by equation (1.1) [16]:

$$C_e = \frac{\varepsilon S}{d} \tag{1.1}$$

where

S is the surface area of electrode/electrolyte interface;
ε is the dielectric constant;
d is the thickness of electrical double layer.

The working principle of wet IEAP actuators with an ionic polymer membrane doped with mobile cations and plated by metal electrodes is rather well agreed on. When voltage is applied between the electrodes, the mobile cations move towards the negative electrode. As the cations (e.g. Na^+ or Li^+) are practically always in a hydrated state in a water-solution, the water molecules are transported along with them. The excess of cations and water near the negative electrode causes expansion of this surface of the IEAP while the opposite side is compressed [1]. Furthermore, the electric-double layers are formed at the interface of coating electrodes and separator polymer [17]. These processes are registered as the bending of an IEAP actuator. However, the gradual formation of electrical double-layers forces cations to reduce or give up completely their hydrate coating, which escalates to a large amount of water flowing back or out from the electrode. This process is called the phenomenon of back-relaxation in which the IEAP starts moving backwards after being subjected to a constant level of voltage for a certain period of time.

Although the water-based ionic actuators are advantageous for devices in an aqueous environment, for diverse conditions actuators that only operate in a particular working solution are undesired. On the contrary, the so-called dry ionic actuators operate in a dry environment while the surrounding humidity may affect their performance. In the dry ionic EAP actuators usually some specific ionic liquids (IL) are used as electrolytes. Ionic liquids are non-volatile

at room temperature and have a relatively large electrochemical window (e.g. 3.5 V for $EMIMBF_4$) [18]. In addition to dry actuation, the use of ILs as electrolytes has made it possible to utilise purely ion-permeable separators, instead of the *ionic* polymer membranes.

The understanding of the actuation mechanisms for the actuators with carbon electrodes is not conclusive and can be considered a subject of dispute. The major difference of these IEAP actuators in comparison to the previously described case is that both cations and anions are mobile and the separator membrane is not ionic. Baughman *et al.* have proposed a charge injection model where bending is induced by electron injection to an expanding surface and hole injection to the opposite side [11]. On the other hand, Fukushima *et al.* suggested that the bending occurs due to the transport of ions caused by the applied electric stimulus [13]. Typically the cations and anions are of different sizes, thus, upon electrically induced relocation of ions within the composite structure, one surface expands and another one contracts. Additionally, Takeuchi *et al.* pointed out that the accumulated charge of an emerging electrical double-layer between the boundary of carbon particles and the electrolyte, directly contributed to the generated strain of carbon-electrode actuator with ionic liquid as electrolyte [19]. Most likely a combination of all these mechanisms is responsible for bending the actuators with carbon-based electrodes.

In literature, ionic polymer (such as Nafion or Flemion) actuators plated by metal electrodes are often referred to as IPMC (ionic polymer-metal composite) [1,8,20,21]. However, due to the increasing development of new types and architectures for IEAP materials, this term is no longer accurate for all similar IEAP structures. Carbon-polymer composite (CPC) is a fairly new term introduced to distinctively address the materials with carbon electrodes on a not necessarily ionic polymer membrane. However, there are also mixed types of IEAP actuators where the ionic polymer membrane is coated by both carbon and metal layers while ionic liquid is used as electrolyte [22], thus, challenging the clear distinction between IPMC and CPC.

As this thesis is focused on analysing the role of electrode material and using its properties for sensing position and/or curvature of an IEAP sample, a more detailed description of variety of electrode materials is provided in the following section.

1.3. Electrodes of IEAP

The state of art IEAPs of multilayer structure are created with electrodes of three main types: metals, different allotropes of carbon, and conducting polymers.

From the perspective of actuation, electrodes and their fabrication techniques must meet certain mechanical and electrical requirements. In order to foster actuation, the electrodes must be compliant and provide good electrical conductivity [23]. Furthermore, a large interfacial layer is required between the electrode and separator membrane to maximise the electrochemically active

surface area [15] and adhesion [8]. The electrodes must form a uniform chemically and mechanically stable conductive layer [8]. Even the anisotropic surface roughness affects the actuation properties, e.g. electrodes with crosswise grooves or cracks improve the performance of an IEAP actuator [24].

By using chemical electroless plating for depositing metal (such as platinum (figure 1.2) or gold) onto an ionic polymer membrane, interpenetrating metal electrodes are attained. As the metal particles interpenetrate into the polymer membrane, a high interfacial area between the polymer film and metal electrode is achieved. However, as the bending motion is achieved due to stretching of the polymer backbone, the metal electrodes become cracked (figure 1.2), which reduces their electronic conductivity and causes leakage of mobile ions and solvent in and out of the IEAP laminate.

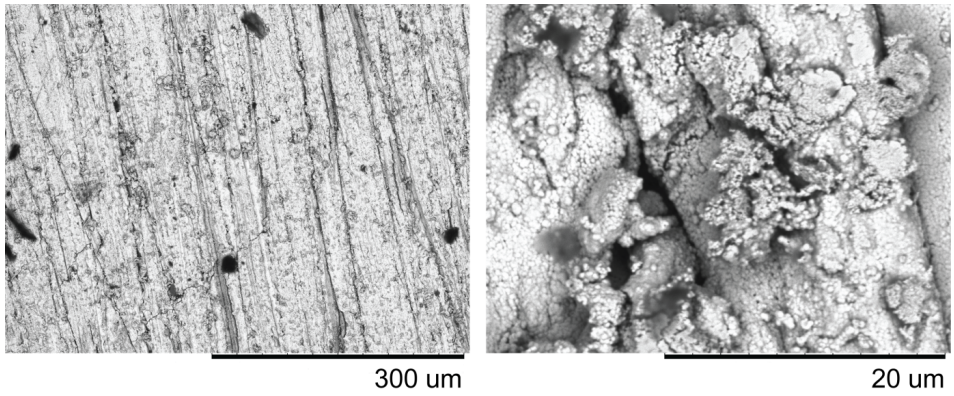

Figure 1.2. Top-view of a chemically plated platinum electrode.

Although the noble metals (e.g. gold and platinum) are most often used as electrode materials for ionic polymer actuators [25,26], several authors have successfully demonstrated the use of non-precious metals such as copper [23,27–29]. In these cases, by means of electroless plating copper and platinum are jointly deposited on Nafion. One of the challenges of using copper-based electrodes is the rapid oxidation process which will quickly reduce the electronic conductivity of an electrode.

In the long line of creating electrodes from a variety of metals as well as mixtures of metals, palladium [30,31], nickel [32], silver [31,32], and zinc [33] should also be mentioned.

Akle *et al.* demonstrated that the capacitance of a trilayer system is directly correlated to the magnitude of actuation and proposed a novel 5-layer construction for IEAP actuators [15]. Ionic polymer membrane containing IL was covered by a mixture of Nafion and ruthenium dioxide (RuO_2) powder. RuO_2 has a very high specific surface area, thus, providing high capacity (e.g. 1 F/cm^2) for the charge accumulation on the electrode. The additional layer

of gold placed on top of RuO_2 further improves surface conductivity. In order to achieve such a structure, the standard chemical methods were discarded and a novel direct assembly process (DAP) was introduced [14,34,35]. DAP involves hot-pressing individually prepared layers into one multilayer composite structure [35].

As an advancement for this dry 5-layer construction of IEAPs, Palmre *et al.* showed that similarly to RuO_2 enhanced performance of an actuator can be achieved with nanoporous carbon (e.g. carbide-derived carbon or carbon aerogel) casted as an intermediate layer between Nafion and gold (figure 1.3) [22,36].

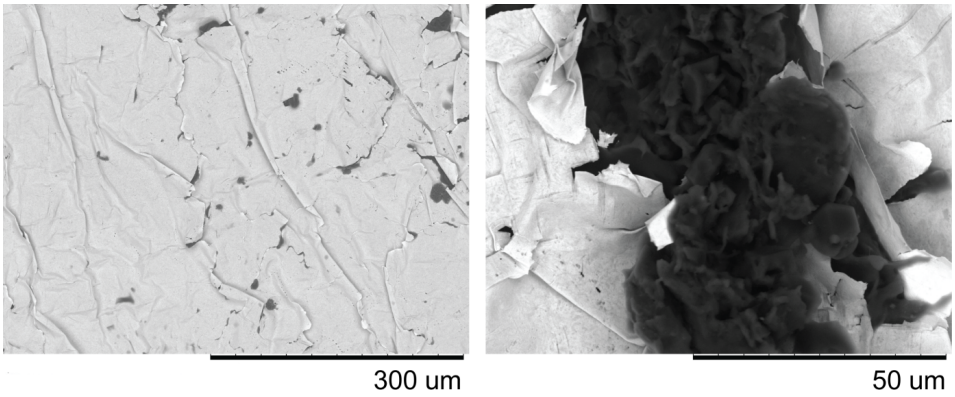

Figure 1.3. Top-view of a carbide-derived carbon electrode with thin gold layer.

There exists a notable amount of research papers reporting on the enhancement of the performance of ionic polymer actuators by adding different carbon allotropes (e.g. nanotubes [37–39], fullerenes [40], graphene [41], graphite [42], carbon black [34], etc.) into the composition of polymer membrane and/or electrodes.

However, the original idea of creating metal-free ionic actuators with carbon electrodes comes from Baughman and co-workers [11]. In addition to implementation of CNT electrodes, a use of non-ionic polymer was adopted, *i.e.* it was demonstrated that pure carbon nanotube electrodes on a PVC membrane constitute a bending ionic actuator when submerged in aqueous electrolyte of NaCl [11].

The concept behind the contribution of porous carbon to the electroactivity of a material is related to the electrical double-layer emerging at the boundary between carbon and electrolyte [19], *i.e.* the surface area of this boundary is of great importance. Therefore, to date, a variety of actuators with electrodes made of carbon allotropes with relatively high specific surface have been developed [13,43–46]. Another key advancement has been the utilisation of ionic liquids that enable the creation of actuators able to operate in diverse environments.

Hence, a typical carbon-based actuator consists of highly porous carbon electrodes separated by electronically insulating ion-permeable thin polymer film. The whole structure – electrodes and separator – contains ionic liquid as an electrolyte.

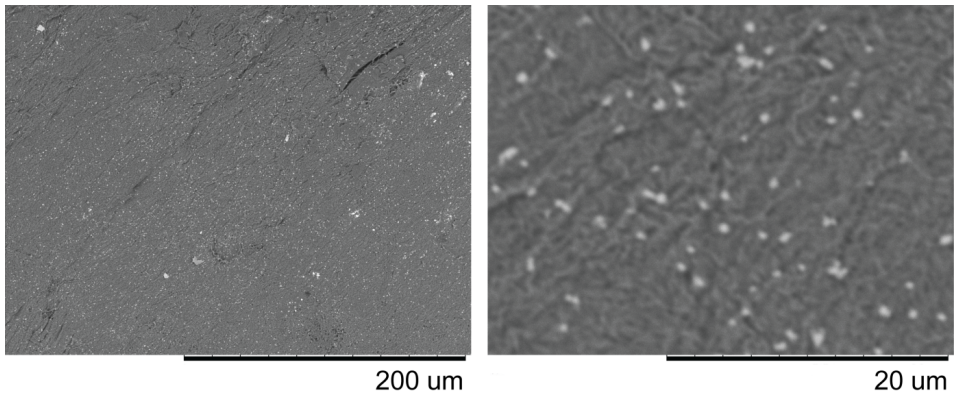

Figure 1.4. Top-view of a bucky-gel electrode with SWCNTs.

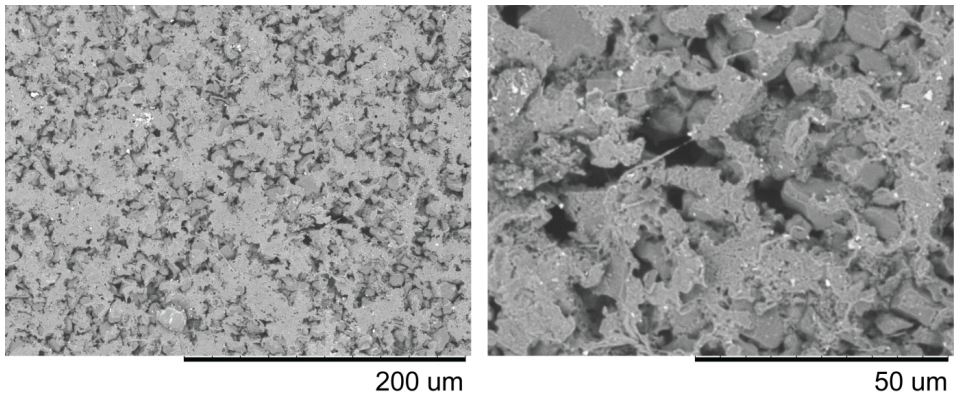

Figure 1.5. Top-view of an electrode consisting of PVdF(HFP), IL, and CDC.

Fukushima *et al.* reported an ionic actuator with so-called bucky-gel electrodes (figure 1.4) consisting of single-walled carbon nanotubes (SWCNT), ionic liquid and poly(vinylidene fluoride-co-hexafluoropropylene) (PVdF(HFP)) [13]. Subsequently it was shown that electrodes of such an actuator can also be created without the component of binding polymer by using millimetre-long SWCNTs [43]. Moreover, in combination with binding polymer and IL, using carbide-derived carbon (CDC) or carbon aerogel as an electrode material has also been successfully demonstrated for both linear and bending actuators (figure 1.5) [44–46].

1.4. IEAP as sensor

Practically every flexible IEAP also exhibits the mechanoelectrical transduction property [3,47–49], which is typically explained by a reverse actuation mechanism. The external manipulation of an actuator causes dislocation of mobile ions which is detected as a short-circuit current or open-circuit voltage between the electrodes. However, when constant curvature is externally imposed to an IEAP sheet, the sensing signal decays as the ion distribution balances [3,49].

At least two principally different sensorial effects can be described for the ionic polymer materials. A conventional ionic polymer sensor with metal electrodes can be explained by a mechanism of reverse actuation [3,21]. External mechanical manipulations of a sample yield a dislocation of mobile ions within the polymer-membrane. The resulting unbalanced allocation of ions can be detected as a low level electrical signal between the opposite metal electrodes of the IEAP [3,20,21,47,50]. However, the signal will dissipate as the uneven concentration of ions evens out. Therefore, this type of sensor is typically used for energy harvesting or motion detection while quantitative sensing of the position is somewhat challenged.

In order to utilise metal-plated IEAP as a position sensor, Punning *et al.* demonstrated that the resistance of metal electrodes of IEAP are strongly correlated to material curvature [51]. This effect is caused by the inhomogeneous nature of electrode material that is cracked due to deformation of the laminate. When material is bent, expansion of the electrode causes noticeable increase in its resistance, while only a slight decrease of resistance is observed on the compressed electrode [51]. This phenomenon is based on the idea that as the length of a conductor increases the electrical resistance of the material also rises. This type of sensor can more easily be used as a position sensor because the resistance of the electrode is directly related to the curvature of an actuator.

The sensorial properties of carbon-polymer laminates have been reported for SWCNT- as well as CDC-containing composites [48,49]. The reported sensors can foremost be implemented for motion detection and energy harvesting as the electrical signal is caused by dislocation and/or re-orientations of ions [49]. Hence, the sensing signal quickly dissipates while constant curvature is imposed to the CPC laminate.

2. MOTIVATION

For their unique characteristics (e.g. straightforward construction, easy customisation, noiseless operation, sensing capabilities, etc.), all electromechanically active materials are considered attractive for biomimetic robotics, biomedical lab-on-chip applications, space technology, etc. [52–54]. In general, ionic EAPs are preferred for their low operating voltage, while distinctive to carbon-based actuators are the benefits from metal-free composition.

However, in order to utilise smart material actuators in a real-life application, one must find a suitable technology for closed-loop control of the actuator. To date, the most typically implemented feedback sources for ionic EAPs are laser displacement sensors [19], video cameras [55], load cells [56], mechanically coupled smart structures [57], etc. Using such feedback devices can, due to their size, cost and complexity, remarkably limit the practical application areas of EAP actuators. It is thus desirable to avoid unwieldy off-board sensors for closed-loop control.

Some of the more sophisticated feedback systems for ionic EAPs include use of other smart transducers coupled with the actuator. For example, Leang *et al.* mounted a strain gage on an IEAP electrode to track the movement of the actuator [58], while Chen *et al.* have demonstrated stacking a piezoelectric PVdF on a metal-plated ionic actuator [57,59]. Similar concepts have also been developed that mechanically couple sensing and actuator strips side by side, instead of stacking [60–62]. The complications related to such systems include electrical cross-talk from actuator to sensor and diminished actuator performance due to a passive sensing element.

Another prospect for achieving closed-loop control of an ionic EAP actuator is utilising simultaneously the material's actuation and sensing properties. Such a system, where feedback on instant displacement is acquired from the actuator itself, is called self-sensing, and it is widely reported for a diverse selection of smart material actuators [7,63–66].

While IEAPs are similar in construction and operation, their working mechanisms should be considered different. As carbon-based IEAP (cIEAP) are roughly 10 years younger than the ones with metal electrodes (mIEAP), the level of understanding about the functional principles is also varied. Therefore, this thesis aims to implement what is known about metal-plated ionic polymer transducers on carbon-based actuators. By such a comparison between these two materials, the similarities and also differences become clear.

The objective of the current thesis is to compare metal- and carbon-based IEAP actuators and to develop an electrical transmission line model in a form of equivalent circuit for cIEAP actuator (chapter 3 and paper I) with a possible use as a self-sensing actuator (chapter 4 and paper I). Another goal of this work is to develop reliable self-sensing ionic actuators – self-sensing IEAP devices are proposed, analysed, and modelled in chapters 5 and 6 (papers II and III).

3. ELECTROCHEMICAL IMPEDANCE SPECTROSCOPY OF IONIC ELECTROMECHANICALLY ACTIVE POLYMERS

3.1. Introduction

Multilayer IEAP actuators used in this research are complex systems composed of mobile ions, solvent and carbon or metal electrodes in a sophisticated structure. Both conductive and isolative components are integrated: while electron conductance is present mainly in electrode layers, ions can move throughout the IEAP.

As the structure and chemical composition of an IEAP material is defined by the fabrication process, it is not conclusively clear how these components interact with each other in the sense of electrical signals. In order to obtain a thorough understanding of the internal mechanisms of an IEAP, electrical impedance spectroscopy (EIS) is utilised.

In a standard DC or single frequency configuration, it is difficult to identify the different contributions of the current. The EIS technique is considered a powerful tool that can often discriminate all these different contributions on the basis of their respective time constant. Moreover, EIS allows characterisation of IEAP by a lumped equivalent circuit made up of resistors, capacitors, and possibly inductances. This chapter implements EIS to the electrode layers of two IEAP structures for the purpose of determining the electrical model of a cIEAP actuator that can explain some of the processes occurring on the electrode in the course of bending.

There exists a variety of models describing mIEAP actuators and sensors in the form of an equivalent circuit. These models can roughly be divided into two categories: lumped and distributed. While distributed models typically exhibit very good precision, they are complex and thus time-consuming for real-time application. Lumped models, however, compensate their lack of precision with good readability and straightforward calculations.

Lumped equivalent circuits often depict IEAP as a RC-circuit with relatively small amount of capacitors and resistors [67–70]. Figure 3.1 depicts two different examples of lumped models proposed for mIEAP actuators.

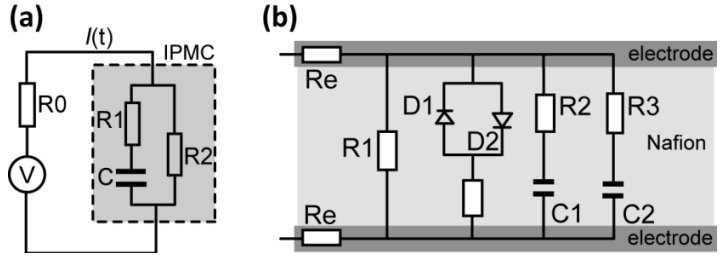

Figure 3.1. Lumped models for metal-plated IEAP. a) Model by Bao *et al.* [67] b) Model by Bonomo *et al.* [68]

The basis of the distributed models of an mIEAP was proposed by Kanno *et al.* [71]. In this model the conductivity of the electrodes is described by a series of resistive elements and the capacitive and the conductive properties of the ionic polymer incorporating the mobile cloud of ions is described by parallel capacitive and resistive elements. This model is refined by several authors. Shahinpoor and co-workers added to the model an unknown intricate impedance caused by charge transfers near the electrodes [23]. Chen and Tan describe a control-oriented dynamic distributed model for mIEAP actuators [72]. Takagi *et al.* present a distributed circuit model of mIEAP by non-rational transfer functions [73]. Punning *et al.* describe a similar model by partial differential equations [74]. Collectively, the distributed models treat the metal electrode layers of a mIEAP as a pure resistance and the polymer layer as a kind of impedance. By specifying the elements of electrode also to impedance, a generalised distributed model can be represented as depicted in figure 3.2. This generalisation takes into account the possible capacitive nature of electrodes.

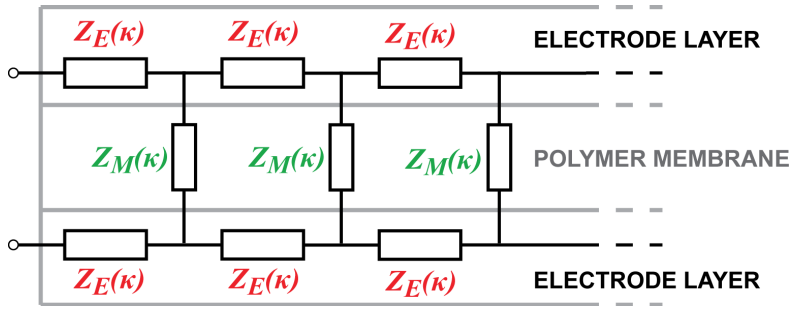

Figure 3.2. Generalised distributed equivalent circuit of ionic EAP.

The goal of this chapter is to determine the equivalent circuit of a cIEAP actuator in the form of a transmission line, similar to that presented by Punning *et al.* [74]. It consists of an infinite series of similar infinitesimally short equivalent circuits with discrete elements. As it is later demonstrated, in order to describe an accurate electrical model of a carbon-polymer laminate it also becomes necessary to investigate the properties of the components that make up the cIEAP actuator. This approach is, however, challenging for chemically created mIEAP actuators.

In this chapter, by means of electrical impedance spectroscopy, a relation between the shape of an IEAP actuator/sensor and its electrical parameters (resistance, impedance, and capacitance) is described. By extending the idea behind a distributed model of a mIEAP transducer [74], an equivalent circuit in the form of a transmission line is proposed for a carbon-polymer actuator, thus, providing extensive and comparative study between these two types of materials. Such comparison helps better to grasp the mechanisms of carbon-

based materials as the *a priori* well-studied metal-plated ionic actuators can be considered to be a reference.

Detailed understanding on which electrical parameters are dependent on material bending and describing this correlation is essential for designing sensorial and self-sensing systems. The experiments described in this chapter study the two types of EAPs independently by using the EIS equipment, while different degrees of bending are imposed to the composite material, summarising with a reasonable equivalent circuit for carbon-polymer composite.

3.2. Experimental

The curvature (denoted by κ and defined as inverse radius r, *i.e.* $\kappa = 1/r$) of a bent IEAP is directly related to the displacement of one (*i.e.* moving) tip of the actuator, since in the cantilever configuration, the other end of the material always remains fixed. The desired curvature was externally imposed to the IEAP actuator by means of a special rig that allowed varying the curvature of the material in the range of 15 to 100 m^{-1} (figure 3.3). This rig forces the IEAP sample to follow relatively uniform curvature which is most often considered as best approximation to describe the actuator's bending.

Figure 3.3(a,b) depicts a multilayer IEAP sample in this customised rig which is enforcing different degrees of curvature. The system allows application of consecutive curvatures to this sample; however, measurements of straight samples cannot be carried out in this type of setup. Figure 3.4 presents the mechanics of a multilayer IEAP: as the material is bent, the bottom electrode is notably compressed and the top one expands (figure 3.4(b)). In order to measure the effects due to compression and extension of the same electrode layer, the sample has to be taken out of the system and turned around.

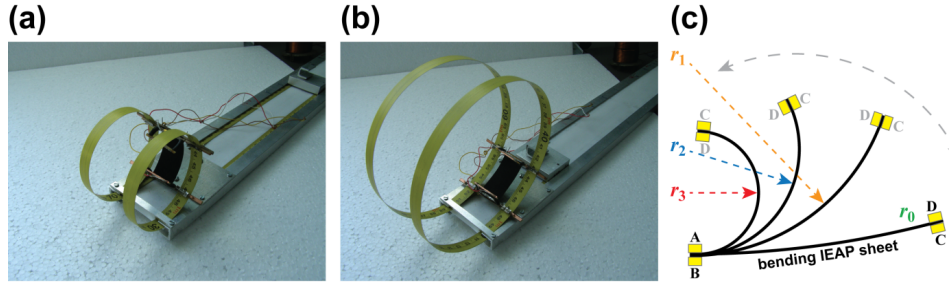

Figure 3.3. Experimental setup for measuring electrical impedance in respect to the curvature of a material.

In the course of experiments the IEAP sample was fixed to the rig with four terminals, thus allowing measurements of all necessary signals between the two electrodes as well as along the electrode layers. While different curvatures were enforced to the sample, the cross-electrode impedance was measured between terminals A and B (figure 3.3(c)), and the corresponding measurements for electrode layers were conducted between terminals A and D, or B and C respectively. Terminals B and C represent the signals registered from the electrode that undergoes expansion and this convexity of an electrode is expressed as the negative curvature. The compression of the electrode layer is identifiable as the positive curvature (figure 3.4).

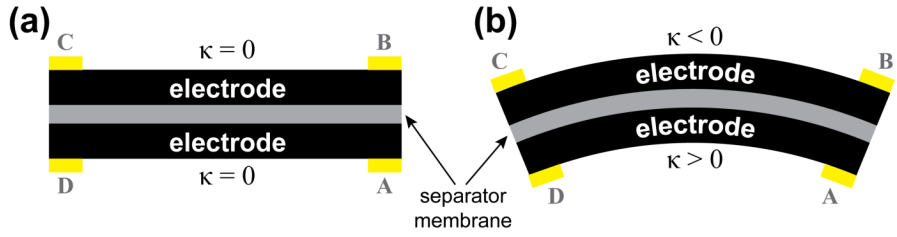

Figure 3.4. Bending mechanics of a multilayer IEAP. (a) Initial state of a trilayer IEAP; (b) Bending of a trilayer IEAP.

A PARSTAT 2273 potentiostat from Princeton Applied Research was used for EIS measurements at a voltage level of 40 mV in the frequency range of 10 mHz –100 kHz. The low voltage that was selected will not cause significant bending of the actuator, nor does it generate any faradic processes that could deteriorate the integrity of the electrolyte.

In order to interpret some properties of studied materials, apparent capacitance $C(\kappa)$ is defined as the capacitive response of the IEAP system that is considered a black box. It is calculated from the empirical EIS data using equation (3.1) without any regard to the actual origin of this capacitive effect.

$$C(\kappa) = \frac{1}{\omega Z_C(\kappa)} \tag{3.1}$$

κ is the curvature of the IEAP sample;
ω is the angular frequency;
Z_C is the complex part of impedance that is considered completely due to the capacitance.

Two types of ionic EAP materials are studied in this chapter: ionic metal-polymer composite (IPMC) and carbon-polymer composite (CPC) (table 3.1). While in some cases it can be challenging to explicitly distinguish between CPC and IPMC materials, the samples investigated in this thesis can be clearly categorised to either CPC or IPMC. Therefore, hereinafter these acronyms are used to code the materials outlined in table 3.1.

The IPMC material used for these experiments was a Musclesheet provided by BioMimetics Inc. It is a water-containing proprietary ionic polymer membrane with Na^+ cations and platinum as electrodes. This material is used exclusively in deionised water.

The CPC is composed of boron carbide-derived carbon with a specific surface area of 1,800 m^2/g, poly(vinylidene fluoride-co-hexafluoropropylene) – PVdF(HFP) – as binding polymer and separator, and 1-ethyl-3-methylimidazolium tetrafluoroborate ($EMIMBF_4$) as the ionic liquid. This material was prepared in-house and a more detailed description of the preparation process of such actuators is given by Torop *et al.* [45]. Experimentation with this carbon-coated IEAP is carried out in an air environment.

Table 3.1. Description of IEAP materials studied in this chapter.

	IPMC	CPC
Separator membrane	Nafion (ionic)	PVdF(HFP) (ion-permeable)
Separator thickness	~200 µm	~30 µm
Electrode composition	platinum	carbide-derived carbon and PVdF(HFP)
Electrode thickness	10–20 µm	~150 µm
Solvent	deionised water	ionic liquid $EMIMBF_4$
Mobile ions	Na^+	$EMIM^+$ BF_4^-
Electrode-deposition method	chemical plating	direct assembly: layer by layer casting and hot pressing
Working environment	deionised water	air

3.3. Correlation between the curvature and the impedance of a whole IEAP

Cross-electrode impedance for both types of IEAPs indicate a large component of capacitance (*i.e.* the linear rise in figure 3.5(a)), especially at lower frequencies, which is shown to be a significant contributor to the actuation properties of an EAP material [15]. While the cross-electrode impedance can present some type of correlation to curvature, the phenomena is directionally independent and relatively small [75] (see also **I**).

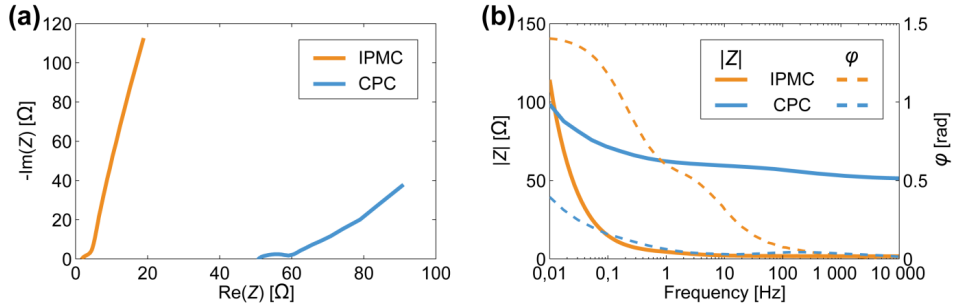

Figure 3.5. Nyquist and Bode plots for cross-electrode impedance of IPMC and CPC samples.

Such electrochemical systems as described in figure 3.5 are often fitted to Randles circuit (figure 3.6) consisting of a parallel combination of double-layer capacitance and charge transfer resistance in series with an active electrolyte resistance; diffusion is described by a Warburg element.

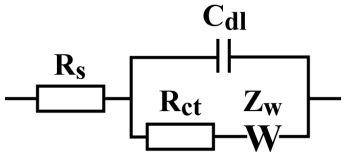

Figure 3.6. Randles circuit, R_s – active electrolyte resistance, C_{dl} – double-layer capacitance, R_{ct} – charge transfer resistance, and Z_W – Warburg element

Cross-electrode impedance of a CPC exhibits a slightly flattened semicircle (figure 3.5(a)) that is typically interpreted as a parallel combination of capacitive and resistive components (figure 3.6). The steep rise in the imaginary part of Z indicates a strong capacitive response of the system together with a diffusional process. These results comply well with the measurements conducted on another type of CPC device – a bucky-gel SWCNT actuator [76,77]. For IPMC,

the capacitive response and diffusional process are also well-visible while active electrolyte resistance (figure 3.6) is extremely small.

It is clearly dominant in figure 3.5 that both studied composite structures exhibit extremely large capacitance due to ion transportation. This phenomenon is observed as the nearly linear rise in the Nyquist plots (figure 3.5(a)). Similar graphs are often registered for electrical double-layer supercapacitors with porous electrodes [16]. This linear rise is interpreted by means of a gradual formation of electric double-layers: ions penetrate deeper into porous electrode, thus increasing the capacitance of the system [16]. Additionally, as mentioned earlier, the slightly flattened semi-circle, especially in the case of a carbon-based actuator, indicates to a capacitor and resistor in parallel. The absence of such a semi-circle in the Nyquist plot for IPMC (figure 3.5(a)) can be explained by relatively high resistance in parallel with the capacitance.

The results of EIS measurements, conducted on one electrode of the whole IEAP composite structure are depicted in figures 3.7 and 3.9. These data lead to two conclusions:

1) the impedance measured from the electrode layer is correlated to the IEAP curvature;
2) in the implemented frequency range different mechanisms are registered for IPMC and CPC.

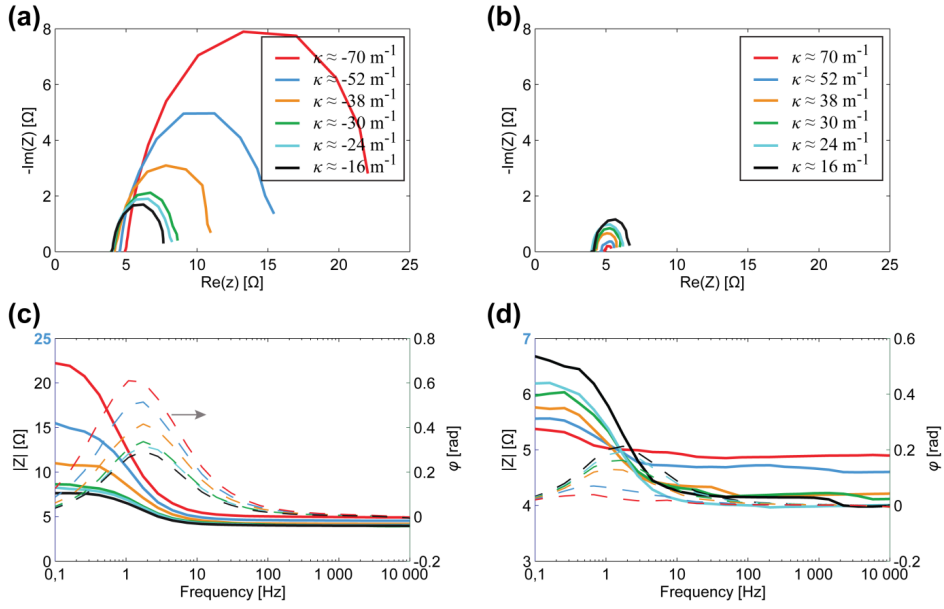

Figure 3.7. The correlation between the impedance of the electrode layer and the curvature of an IPMC. (a) Nyquist plot for convex electrode layer; (b) Nyquist plot for concave electrode layer; (c) Bode plot for convex electrode layer; (d) Bode plot for concave electrode layer.

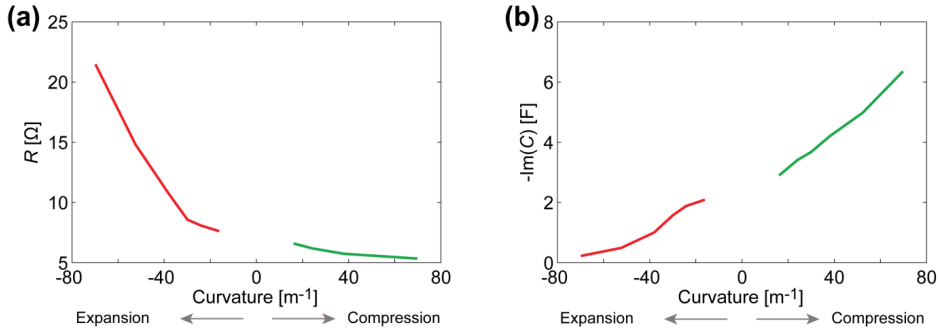

Figure 3.8. (a) The correlation between the resistance of the electrode layer and the curvature of an IPMC at the frequency of 0.2 Hz; (b) The correlation between the apparent capacitance of the electrode layer and the curvature of an IPMC at the frequency of 0.2 Hz.

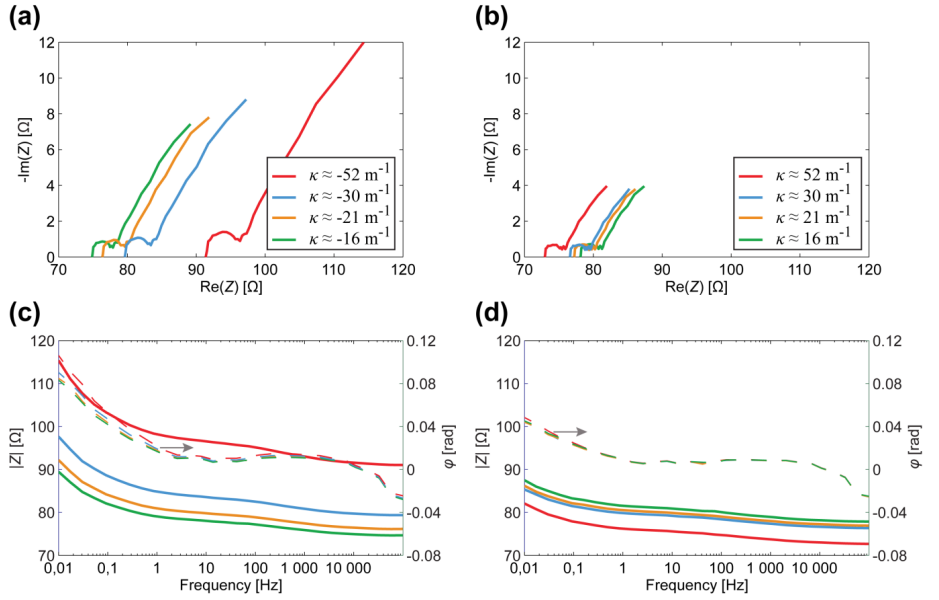

Figure 3.9. The correlation between the impedance of the electrode layer and the curvature of a CPC. (a) Nyquist plot for convex electrode layer; (b) Nyquist plot for concave electrode layer; (c) Bode plot for convex electrode layer; (d) Bode plot for concave electrode layer.

The semi-circle in figure 3.7(a,b) points to a parallel combination of resistance and capacitance, which for IPMCs can be explained by cracks between the shreds of platinum. It is known that Pt electrodes contain cracks (figure 1.2), thus, the structure of these electrode layers can be considered as an assembly of

side-by-side and/or overlapping metal shreds. In the initial state of IPMC, these shreds of Pt are mostly in contact with one another forming a highly conductive path, although some capacitive gaps also exist in parallel. The alteration of impedance in the direction of both horizontal and vertical axes of the Nyquist plots (figure 3.7(a,b)) is evidence of simultaneous changes occurring in parallel resistance and capacitance of the system. When IPMC is bent, shreds of Pt are pulled apart within the expanding electrode, thus, the touching area of metal decreases along with the increase in size and quantity of capacitive gaps. That means electronic charge transfer resistance of an electrode layer increases while the apparent capacitance decreases (figure 3.8). The apparent capacitance is calculated from the impedance data presented in figure 3.7. Moreover, on the electrode layer undergoing compression, an opposite effect is identifiable: metal shreds are forced closer together, thus, reducing the resistance of an electrode while apparent capacitance rises (figure 3.8). However, the series resistance remains practically unaltered (figure 3.7(a,b)).

The results of EIS measurements conducted on the electrode layer of the CPC laminate are depicted in figure 3.9. The visual appearance of these curves is pretty similar to the cross-electrode curves for CPC depicted in figure 3.5, thus, again exhibiting parallel capacitive and resistive components in series with the resistor. However, the Nyquist plots given in figure 3.9(a,b) show that the curves are scaled along both axes as the electrode layer is expanded, whereas during compression the effects along the imaginary axis are marginal. Consequently, both the resistive as well as the capacitive components alter in the course of bending (figure 3.10). Nevertheless, in the case of electrode compression, alteration along the horizontal axis is more distinct than of the vertical axis (figure 3.9(b)). A clear distinction from IPMC comes from the alteration of series resistance, which is observed as the shifting of the curve along the real axis of impedance in Nyquist plots for both expansion and compression of electrode layer (figure 3.9(a,b)). The structure of the electrode is also completely different for CPC and IPMC as the electrode of a CPC consists of several layers of porous carbon particles bound together by PVdF(HFP) (figure 1.5).

Figure 3.10(a) depicts the relation between the curvature and the electrode layer resistance of a CPC actuator. Similarly to Pt-plated IPMC actuators [51], when a carbon electrode is stretched, its resistance increases noticeably, while the decrease in resistance of the compressed electrode is relatively small.

Based on the above described results, the electrode layers of IPMC and CPC indicate to a strong capacitive element in parallel with resistance. However, at this stage the EIS measurements of the cross-electrode impedance and the electrode layer described above cannot lead to a unique definition of the impedances Z_E and Z_M depicted in figure 3.2. In the case of a distributed circuit, the appearing capacitance can lie in the electrode as well as in the membrane. The appearing altering impedances described above can be explained in many different possible combinations of curvature-dependent capacitive and resistive components of Z_E and Z_M. One sophisticated combination, proven by electronic circuit simulation software, is presented in figure 3.11.

One possible source of indeterminacy for a trustworthy equivalent circuit is the so-called apparent capacitance measured from the electrodes of IEAPs. While capacitive elements of a separator membrane are established by general knowledge of these materials, the IEAP configuration and EIS experimental setup cannot exclusively lead to definite elements of capacitance within the electrode. It is possible that the apparent capacitance measured form the electrode is mainly caused by signal reflection from the opposite electrode via capacitive coupling of the separator membrane.

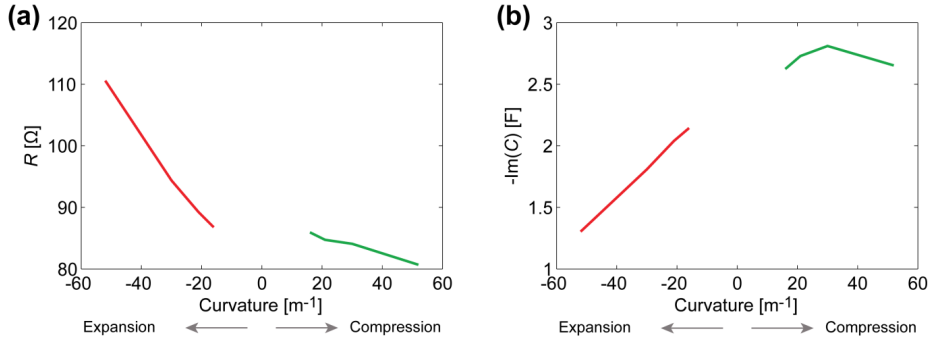

Figure 3.10. (a) The correlation between the resistance of the electrode layer and the curvature of a CPC at the frequency of 0.2 Hz; (b) The correlation between the apparent capacitance of the electrode layer and the curvature of a CPC at the frequency of 0.2 Hz.

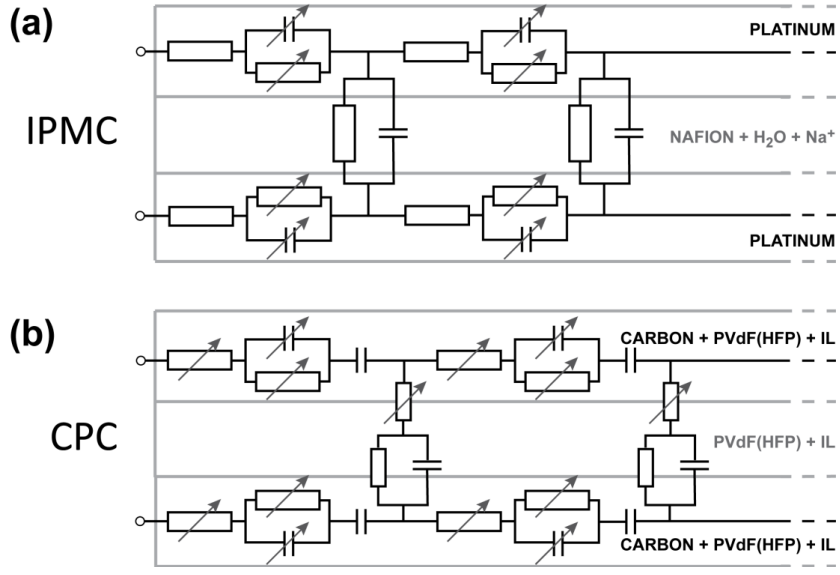

Figure 3.11. Distributed equivalent circuits for (a) IPMC and (b) CPC

3.4. EIS of individual components of a cIEAP

In order to obtain an adequate electrical model of an IEAP actuator, it is beneficial to explore each component individually, *i.e.* to separately test the validity of electrode and membrane circuits given in figure 3.11. Conducting such a study on chemically deposited IPMC material is rather challenging as the electrode is interpenetrated to the membrane and, practically, there is no such thing as separate layers of membrane or electrode. Some researchers even make the distinction of an additional intermediate layer between the separator membrane and electrode [8] of a chemically deposited mIEAP. However, since the cIEAP material is fabricated in-house and the layers of this actuator are created separately and assembled by means of direct assembly process, it is possible to study the components – membrane and electrode – independently.

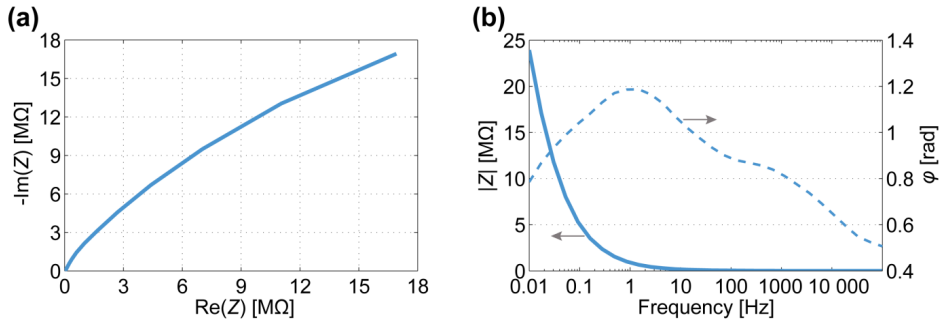

Figure 3.12. Impedance plots for PVdF(HFP) containing IL.

The PVdF(HFP) in a dry compact form is a good insulator but as the separator membrane for IEAP, it is porous and contains ionic liquid. In these measurements, no pure resistance was registered (even in the high frequency range) for such IL-containing PVdF(HFP). The impedance data (figure 3.12) on 30–50 µm thick PVdF(HFP) membrane containing IL, shows only mass transportation (in this case ion transportation) effect.

Therefore, corresponding distributed and lumped models able to describe such behaviour can be represented as in figure 3.13.

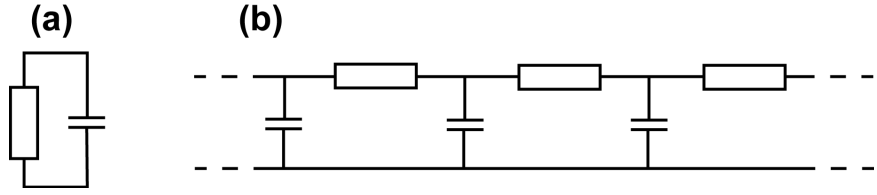

Figure 3.13. (a) Lumped and (b) distributed models for PVdF(HFP) membrane containing IL.

In order to characterise the correlation between the impedance and curvature of a CDC electrode, the electrode was bonded to a thin poly-carbonate film (figure 3.14). In this configuration the impedances of the membrane and the opposite electrode will not interfere with the measurements. Connecting the electrode to a lengthwise inelastic plastic ensures that in the course of external bending the electrode behaves like a regular IEAP. That is, the electrode gets compressed when $\kappa > 0$ and stretched when $\kappa < 0$, and in comparison to signals measured from the surface of a carbon-based IEAP laminate (figure 3.9), any phenomenological difference in results can, thus, be contributed to the opposite electrode and/or separator membrane. In other aspects the experimental setup was the same as described in section 3.2.

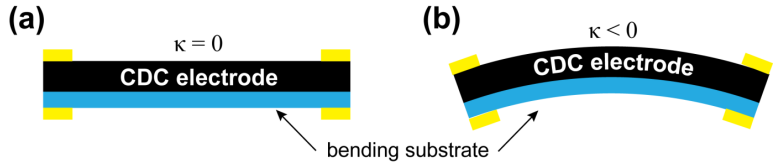

Figure 3.14. (a) Initial state of a CDC-based electrode; (b) Bending of a CDC-based electrode.

Figure 3.15 depicts the EIS data registered from the CDC-based electrode (containing ionic liquid and polymer) in case of different degrees of curvature.

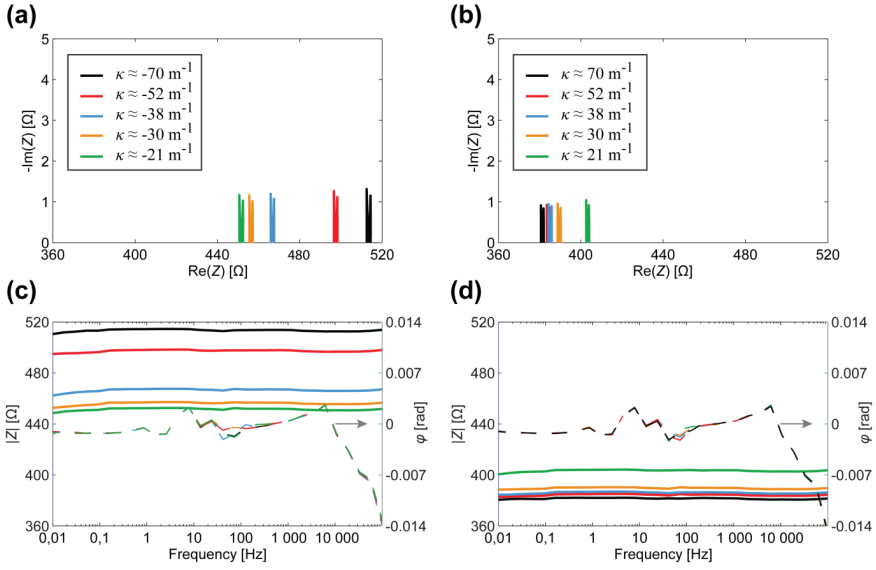

Figure 3.15. The correlation between the impedance and the curvature of a CDC-based electrode. (a) Nyquist plot for convex electrode; (b) Nyquist plot for concave electrode; (c) Bode plot for convex electrode; (d) Bode plot for concave electrode.

The results show that there is no considerable capacitance present in the electrode and demonstrate a clear correlation between the magnitude of impedance and the curvature of a bent electrode. The resistance of the electrode increases considerably during stretching while it lessens only slightly when the electrode gets compressed. The change of resistance can be explained by means of the touching surfaces of CDC particles: the concentration of CDC particles in the electrode is high enough to ensure pure electronic conductivity. When the already compact electrode gets more compressed, the touching surface of CDC particles increases a little, resulting in the rise of conductivity. When an electrode is stretched, some carbon particles are disconnected from each other, leading to a decrease in conductivity.

No relevant capacitive or inductive effect is detected from the CDC-based electrode. The absence of capacitance becomes clearer from the cyclic voltammetry of the same sample given in figure 3.16. Despite implementing a wide range of sweep rates (50 $mV \cdot s^{-1}$–2 $V \cdot s^{-1}$), the voltammogram remained linear, and the only parameter affecting its slope is the curvature of the electrode. This indicates that the concentration of CDC particles in the electrode is high enough to not cause any cavities in the conducting layer, even when stretched. Therefore, purely electron-conducting effects are registered in the CDC-based electrode.

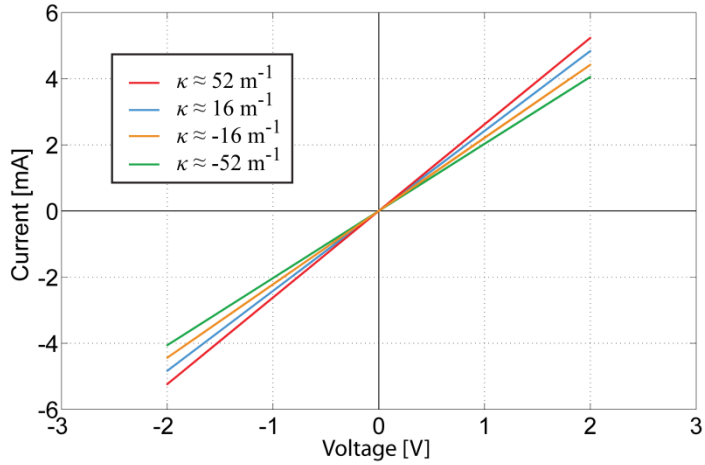

Figure 3.16. Voltammogram of a CDC-based electrode for different material curvatures.

3.5. Discussion and conclusions

The experiments described in section 3.3 showed the presence of capacitive elements in the membrane as well as in the electrodes. Now, based on the above described results, we can adjust the components and eliminate capacitance from the electrode. The resulting distributed equivalent circuit of CDC-based IEAP is depicted in figure 3.17. The impedance of the electrodes Z_E stands for pure

resistivity, while the impedance of the membrane Z_M consists of capacitive and resistive elements in parallel. This leads to the understanding that the apparent capacitance in figures 3.9 and 3.10 is registered only due to the coupling effect of the separator membrane. Despite this deduction, the described capacitive phenomenon can still be implemented when using this material as a black-box position sensor.

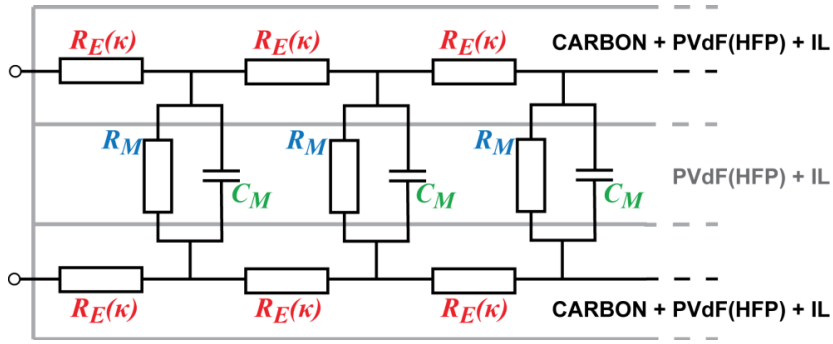

Figure 3.17. Distributed equivalent circuit for IEAP with CDC electrodes.

In this chapter it was shown that impedance measured from an electrode of the IEAP is subject to change in accordance to the curvature of the material. This relation involves alteration in both resistance and apparent capacitance; however, the EIS study on a single carbon-based electrode exhibits no relevant capacitive effects. Therefore, only resistive elements are considered to make up the electrode in a distributed equivalent schematic for carbon-based actuator. The study on metal-based electrodes is inconclusive as the impedance data can either be interpreted to support existing transmission line models or to suggest parallel capacitance in the electrode.

Nevertheless, despite the background phenomena, when measuring signals from the electrode layer of an IEAP actuator, capacitance is well registered and, thus, cannot be neglected when creating applications utilising sensorial effects on the electrode layer. The resulting equivalent circuit (figure 3.17) provides an electrical model for a cIEAP position sensor, self-sensing actuator, and other devices.

4. ELECTRODE SIGNALS OF AN IONIC ELECTROMECHANICALLY ACTIVE POLYMER ACTUATOR

4.1. Introduction

As described in chapter 2 the concept of self-sensing actuator involves using IEAP simultaneously as actuator and sensor, while the sensing signal is used for closed-loop control of the actuator. The self-sensing IPMC that was proposed by Punning *et al.* [65] described a system where signals along the metal electrodes are measured during the actuation cycle. Due to changes in the resistance and apparent capacitance, it may be possible to extract information on curvature.

Punning *et al.* introduced two additions to the conventional cantilever configuration that could aid in realisation of self-sensing IEAP. In order to measure electrode signals, extremely lightweight gold clamp with thin copper wiring was placed to the moving tip of the actuator. Furthermore, it was suggested to compare voltage drops from fixed and flexible states of an IPMC to attain information on bending curvature and/or tip displacement of an IPMC actuator.

In chapter 3 it was demonstrated that the resistance and the apparent capacitance of an electrode layer are in clear correlation to the curvature of the material. However, these effects were measured on electrically inactive samples, *i.e.* no input signal was applied to the actuator. The current chapter proposes that signals from the electrode layer of a CPC actuator can be used to detect fluctuations in the curvature of the material. Therefore, creating a foundation for self-sensing IEAP based on the resistive and capacitive alterations due to changes in curvature. However, here the challenge lies in measuring all or some of the described phenomena in an electrically active sample.

It is theorised that signals from CDC-based electrodes are dependent on curvature of the IEAP even in an electrically active state, *i.e.* when an input signal is applied to the actuator. To further demonstrate the capabilities of such a system, a moving obstruction is introduced to this setup. The role of this obstruction is to deliberately alter the curvature of a bending actuator, thus presenting evidence of collision detection capability during the actuation of a cIEAP.

4.2. Experimental

For the measurements described in current section, an experimental setup comprising a PC with LabVIEW and NI PCI-6120 DAQ card was adopted (figure 4.1).

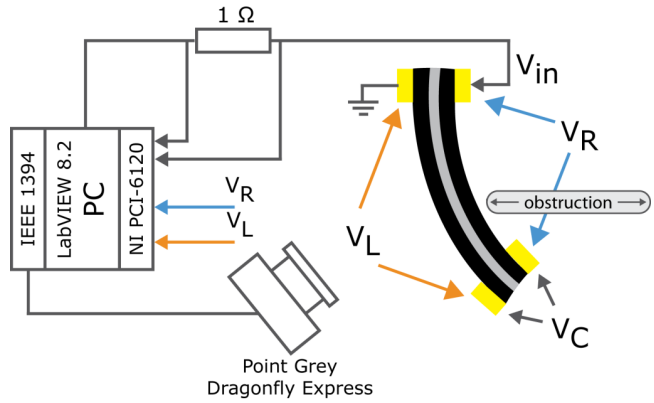

Figure 4.1. Experimental setup.

In these measurements a CPC laminate was placed in a cantilever configuration, as depicted in figure 4.1. In order to register voltage drops along the electrodes, a lightweight clamp with gold contacts was attached to the moving tip of the actuator. The weight of the clamp (less than 100 mg) and the hovering 50-µm-thick wires cause no relevant suppression to the performance of the actuator, capable of lifting several grams [78].

A rectangular driving signal (pulse width of 30 s and amplitude of 3 V) was applied to the CPC actuator. The amplitude of the input voltage was chosen to be within the electrochemical window of the ionic liquid, so no disruptive faradic processes take place between the electrodes, nor inside a single electrode. The actuator driving signal V_{in}, and the voltage drops along the electrodes – V_L and V_R – are measured using the PCI-6120 DAQ board, while the voltage on separator V_C is obtained from the measured results using the arithmetic operations. The NI PCI-6120 features 4 input channels with dedicated 16-bit analog-to-digital converters and 2 output channels with 16-bit digital-to-analog converters for maximum device throughput, and high multichannel accuracy with up to 1 MS/s per channel sampling rates. The large on-board memory delivers reliable data streaming with fewer dependencies on bus availability. Half of the on-board memory is dedicated to analog input and the other half to analog output. The electric current was measured as a voltage drop over a series resistor of suitable value, usually about 1 Ω. The curvature and the tip displacement of the actuator were recorded by a Point Grey Dragonfly Express

camera. Data acquisition frequency was set to 4 S/s while driving signals (V_{in}) were generated at the sampling rate of 1 kS/s.

In the first series of experiments, the bending of the CPC sample was caused by the input driving signal. Continuous movement of the tip occurred for the whole 30 seconds of applied voltage, reaching the displacement of ~10 mm in the direction of the horizontal axis (denoted as Δx in figure 4.2(a)) and ~2 mm along the vertical axis. Another series of experiments were conducted similarly to the previous one but the CPC sample was mechanically fixed to its initial position. This way, despite the applied voltage, the actuator was unable to bend, thus lessening the effects inherent to the alteration of electrode resistance due to the instantaneous curvature of the material. Lastly, experiments where movement of the IEAP was obstructed by an entering obstacle at a random moment during the actuation were also carried out.

4.3. Signals during the work-cycle of a CPC

The signals measured simultaneously between different regions of the CPC in its electrically active state, *i.e.* during a single work-cycle of the actuator, are depicted in figure 4.2. The exponential decay of electric current in figure 4.2(a) implies that the separator between two electrodes can be regarded as capacitance with no or negligible shunting conductivity.

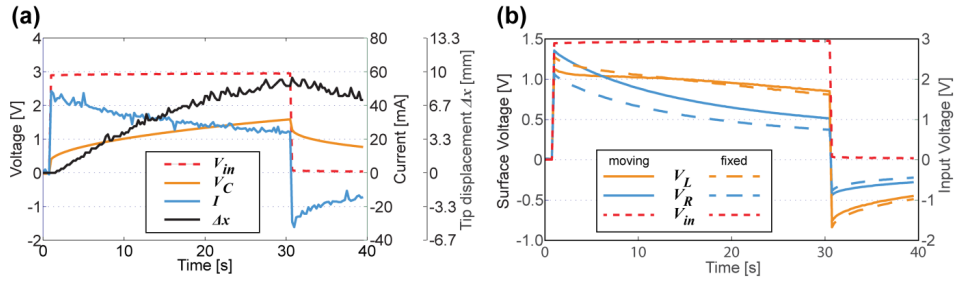

Figure 4.2. (a) Actuator driving signal V_{in}, voltage drop on separator V_C, current I, and tip displacement along the horizontal axis Δx; (b) Voltage drops along the electrodes of the CPC actuator in unobstructed and fixed configurations.

The comparison of voltages along the opposite electrodes of both – unobstructed and fixed actuator – are given in figure 4.2(b). There are two concurrent factors contributing to voltage drops on both electrode layers:

1) signal propagation along the transmission line (dependent on the time constant of the actuator);
2) the time constant is dynamically changing due to the instantaneous curvature of the actuator.

Separating these two processes is a rather complex procedure, however, based on figure 4.2(b) it can be argued that for the extreme cases of obstruction and free movement it is possible to visually distinguish between different signals. Furthermore, the electrode signals of the completely fixed sample describe a particular case where curvature is held constant. This means that the time constant remains unaltered and, thus, measured signals describe only the signal propagation along the CPC as a transmission line.

4.4. Collision detection with a self-sensing CPC

It has been established that resistance and apparent capacitance of an IEAP alter in the course of bending (chapter 3) and to some extent it can be detected during the actuation from the voltage drops on the electrode layers (section 4.3).

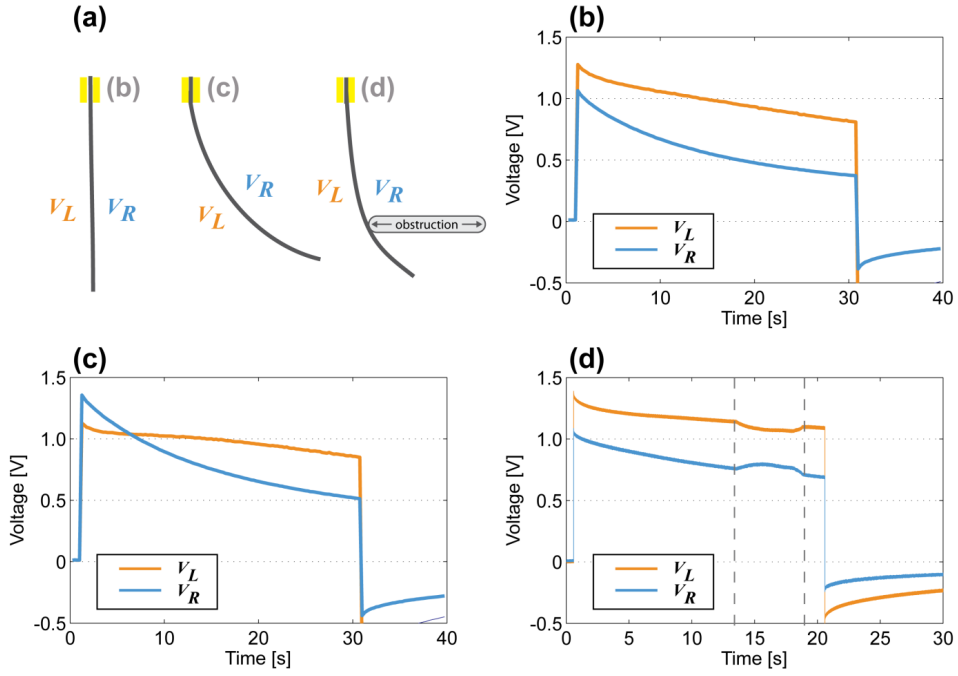

Figure 4.3. a) Curvature of fixed or unbiased, freely actuating, and obstructed CPCs; b) Electrode layers' voltages for fixed CPC; c) Electrode layers' voltages for freely bending CPC; d) Electrode layers' voltages when free movement of the actuator was obstructed at the 14th second of the experiment.

If a CPC actuator collides with an obstruction in its path, a curvature of this actuator may also alter. Figure 4.3(a) demonstrates three geometries for actuator curvatures. Figure 4.3(b-d) depicts voltage drops on electrode layers for each of the three cases for actuator bending represented in figure 4.3(a).

It is explicitly visible that for each case the signals from electrode layers are characteristically different, *i.e.* such a self-sensing CPC actuator can be used to distinguish between free and colliding actuation. One possible application of this type of system can be the creation of biomimetic vibrissae able to detect obstacles in its path.

When the actuator is completely fixed (figure 4.3(b)), the decay of voltage is roughly exponential on each electrode. It is observed from the characteristics that the voltage along the electrodes is distributed unevenly and depends on the curvature of the freely bending actuator (figure 4.3(c,d)). The appearance of a voltage drop along the compressed electrode (V_R) is roughly similar to the previously fixed case. The irregular behaviour of the voltage drop along the stretching electrode (V_L in figure 4.3(c)) indicates that the resistance and apparent capacitance of the corresponding electrode are not constant. Although in chapter 3 it was concluded that no element of capacitance is found in the electrode layer of a CPC, it can be stated that this outcome complies with the fore mentioned results where bending of an IEAP actuator causes a significant change in apparent capacitance measured from the electrode layer that is undergoing expansion (figures 3.9 and 3.10).

Figure 4.3(d) shows voltage drops along each electrode layer of a freely moving IEAP actuator, however in approximately 14 seconds ($\Delta x \approx 5$ mm) an opposing beam forces the actuator back close to its initial state. This impediment is unmistakably visible in voltage drops of each electrode, hence providing a self-sensing collision detecting CPC actuator. Interestingly this phenomenon appears to have a symmetric nature on both voltage drops, which can be interpreted that this effect is not caused only by the alteration of electrode resistance (that behaves differently on compression and expansion (figure 3.10(a)), but instead, by a resultant effect of change in apparent capacitance.

4.5. Simulations of a collision detecting CPC

MATLAB Simulink software was implemented to confirm the above described experimental behaviour with the equivalent circuit proposed in figure 3.17. A model with 5 nodes (single node depicted in figure 4.4(a)) in series was simulated under rectangular input signal (V_{in} = 3 V) for 30 seconds (simulation time step of 0.6 s). During simulation of freely bending CPC (figure 4.4(c)) series resistances R_a and R_b were considered to alter as an exponential function of time (G = 30) because figure 3.10 indicates an exponential correlation between the curvature and the resistance of an electrode. On the other hand, for simulating electrode signals of a fixed CPC (figure 4.4(b)), electrode resistance was kept constant (G = 0). In order to mimic external obstruction (figure 4.4(d)), for a certain period resistances R_a and R_b were subjected to rapid change, *i.e.* G = 20 in the range of 14–21 s, and G = 30 otherwise.

The simulated behaviour of voltage drops along each electrode (figure 4.4(b–d)) corresponds rather well to the experimental results depicted in figure 4.3(b–d).

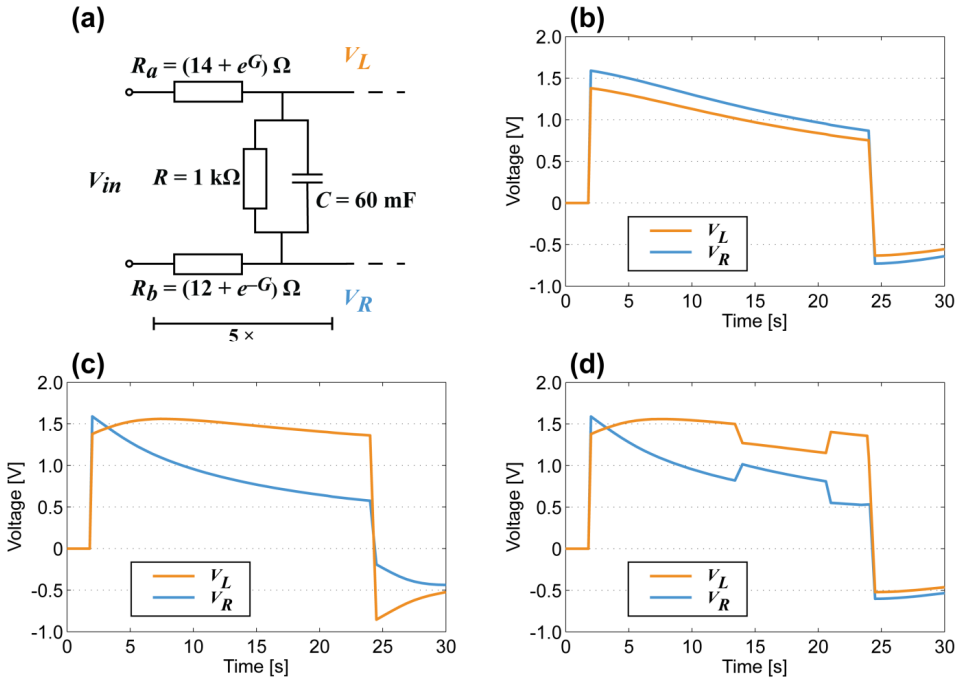

Figure 4.4. Simulation of voltages drops on both electrodes during actuation cycle. a) Single node of simulated circuit and input parameters; b) Output of simulation for fixed IEAP; c) Output of simulation for freely bending IEAP; d) Output of simulation for temporarily obstructed IEAP.

4.6. Conclusions

This chapter implemented the concept of self-sensing IPMC to a CPC actuator. It was demonstrated that by acquiring voltage drops form the electrodes during the actuation cycle, it is possible to differentiate between at least three different modes of actuation:

1) freely bending actuator;
2) completely fixed actuator;
3) obstruction of actuator during bending motion.

Similar results have been previously demonstrated for IPMC, where different voltage drops were acquired in respect to curvature of the actuator [65].

The results also confirm the findings of chapter 3 by demonstrating capacitive and resistive alterations during the work-cycle of the actuator. Therefore, whenever measuring signals from any electrode of an IEAP actuator, one has to consider this capacitive coupling between electrode layers. However, empirical

resistive and capacitive effects are more prominent when measuring the electrode that is being stretched as a result of actuation or external bending. Self-sensitivity of a completely blocked or externally manipulated cIEAP actuator was presented in this chapter. This type of self-sensing system can be utilised as biomimetic vibrissae that allow tactile feedback.

As a result of the simulation it can be stated that the proposed equivalent circuit (figure 3.17) was successfully implemented to estimate the signal behaviour during experimentation. Furthermore, simulation with MATLAB Simulink reconfirms that the signal measured from the electrode layer during actuation cycle is dependent on electrode resistance, which in turn is known to correlate with the curvature of a CPC actuator (chapter 3).

5. SELF-SENSING IONIC ACTUATING DEVICE WITH PATTERNED PLATINUM ELECTRODES

5.1. Introduction

In previous chapters it is demonstrated that carbon and metal electrode layers of IEAPs exhibit a prominent sensorial effect described by either capacitive or resistive correlation to curvature. However, one major complication of creating a fully self-sensing IEAP actuator is related to separating data on curvature from the input signal propagation along the IEAP transmission line. Both of these processes seem to have very similar, if not the same, time constants, thus, precise position control of the actuator becomes rather challenging.

In this chapter, it is proposed to mechanically uncouple sensing and actuation functionality of an IPMC. For that reason, patterning of electrodes is utilised. Patterning is defined as a process where customised grooves are created into the electrode layer.

Many scientific papers adopt patterning of an electrode layer either to create complex actuator mechanisms able to perform MDOF actuation [79–87] or to separate the actuating and sensing functionalities [62,88,89] on one strip of mIEAP.

Jeon *et al.* incorporated patterning into the chemical and electrochemical plating of the ionic polymer by placing a mask of the desired pattern on a polymer before depositing electrodes [83]. However, such processes are time-consuming, have low resolution and often metal particles still permeate the masking tape [83].

The most common methods for electrode patterning are laser ablation [79,80], machining [84,87,89], and manual scraping [62,81,82,88]. Here, the electrode material is removed from a fully functional IPMC to create insulating grooves to the electrode. While such methods are relatively straightforward and provide good precision, often more than just electrode material is removed in the process, therefore weakening the whole structure of the IEAP.

Recently, Rossiter & Mukai proposed two novel methods for patterning the electrodes of a gold-plated IPMC – hot stylus method and electric (or spark) discharge machining [86]. In hot stylus segmentation, the electrode is cut with a high-temperature blade and grooves are generated as a combination of Nafion melting, water vaporising and metal cracking [86]. The spark discharge machining implements the concept of breakdown voltage to remove metal electrodes. The biggest advantage of the hot stylus method is cost-effectiveness, while due to the self-limiting characteristic, the electric discharge machining minimises the amount of removed non-electrode material [86].

Several authors have described attempts to separate the actuating and sensing functionalities by patterning the electrodes [62,88,89]. Those authors utilised the IEAP sensor in a conventional way, *i.e.* as a generating device producing voltage between the metal electrodes. In the current chapter, it is proposed to measure the changes in conductivity of resistive elements patterned

on the electrodes of an IPMC in order to describe the deformation of the actuator-sensor system. Moreover, this patterning is realised coincidently on both sides of the IEAP strip, allowing a differential measurement scheme and, hence, to filter out the effects of common mode noise.

A special design for self-sensing actuator based on a sensory signal acquired from a surface is proposed and patterned to platinum electrodes of an IEAP. Then, selection of techniques for patterning (such as manual scraping, machining, and laser ablation) are tried out and analysed from the perspective of material properties. Proof of concept for such a system is presented along with a straightforward electromechanical model.

5.2. Patterned self-sensing actuating device

The pattern proposed for the IPMC electrodes is depicted in figure 5.1. It consists of three individual segments: a section for the actuating function (*i.e.* the actuator), a shielding electrode to reduce the cross-talk and a sensing element (*i.e.* the sensor). The actuator segment is responsible for bending the whole system. The two sensor electrodes, located at the opposite faces of the strip, bend synchronously with the actuator, while their resistances are in correlation with their bending curvature. The resistances of the sensor electrodes are measured between terminals A–B and A'–B' (figure 5.1). A significant drawback was observed in early versions of the self-sensing system. The device consisting only of sensing and actuating elements exhibits a conspicuous undesired cross-talk effect between the actuator and the sensor parts. The level of crosstalk in the case of a sinusoidal input voltage V_{in} of the actuator part is depicted in figure 5.2. It demonstrates that the voltage V_S between the terminals of the sensor element is strongly correlated with the input current I_{IPMC} of the actuator part.

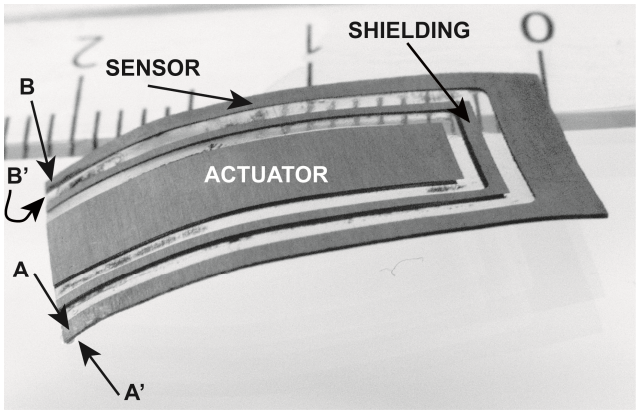

Figure 5.1. Pattern on the electrodes of an IPMC sheet.

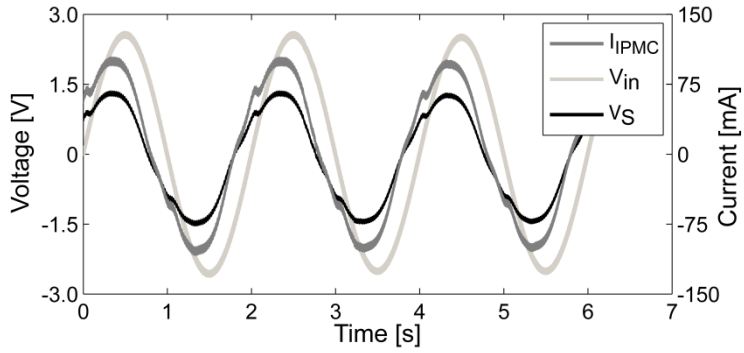

Figure 5.2. The cross-talk between the actuator and sensor parts without shielding. V_S – voltage drop between the terminals of the sensor; V_{in} – actuator input voltage; I_{IPMC} – current through actuator.

Similar behaviour is described by Kamamichi *et al.* [89] who suggested inserting more than one insulating gap between actuator and sensor in order to reduce the electrical cross-talk coupling in IPMCs. As a result, an additional shielding electrode between the sensor and actuator electrodes is introduced. The shielding elements are connected to the system ground in order to suppress further the cross-talk between the actuator and sensor.

Early prototypes of this self-sensing system were created by manual scraping of electrodes with a sharp metal blade. Therefore, the shielding electrodes were unable to remove cross-talk completely. As it is later shown, it was not an issue for machined and laser ablated samples of IPMC. However, to address this matter on manually scraped IPMCs, the sensor electrodes of both patterned surfaces of one IPMC strip were connected in a bridge configuration (figure 5.3). It is assumed that the cross-talk behaves similarly on each surface, *i.e.* it represents a common mode noise. Thus, by adequately connecting the sensors in a bridge configuration, it is possible to subtract such undesired components. Eventually, the bridge configuration increases the sensitivity to the variation of resistance, because the relation between the curvature and the resistance of the two opposite active legs is reversed.

Considering the bridge circuit, two 80 Ω external resistors R are connected in series with each sensor electrode (figure 5.3). It is worth noting that by applying voltage between the sensor electrodes, a motion of the IPMC might be produced. As the voltage of the bridge is applied lengthwise to the opposite sides of the sensor part, the difference of voltage between them is imperceptible at any location and causes no considerable movement of the IPMC actuator. A supply of 1 V provides a sufficiently clear signal to observe the changes in resistance. A straightforward voltage divider circuit was implemented for IPMCs with patterns created by laser ablation or machining.

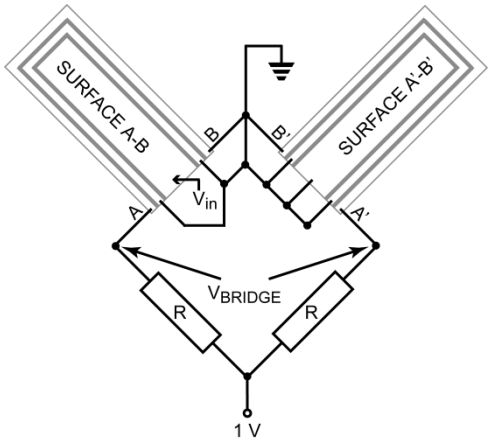

Figure 5.3. Bridge circuit for the measurements of the sensor signals. The two surfaces drawn represent the opposite sides of the same sample of IPMC. V_{BRIDGE} – bridge output signal; V_{in} – actuator input voltage; R – 80 Ω external resistor.

5.3. Design considerations for the bridge circuit

While characterising the relation between material curvature κ and electrode resistance $R(\kappa)$ provides adequate description of sensing capabilities of IEAP material, for technical reasons the performance of bending actuators is often described by tip deflection δ (measured with laser displacement sensor) or strain difference ε between electrode layers [19]:

$$\varepsilon = \kappa t = \frac{2t\delta}{l^2 + \delta^2} \tag{5.1}$$

where t is the thickness of the IEAP sample and
l is the projection of the bent strip on the non-deflected strip.

The underlying principle for equation (5.1) is that in the case of uniform bending the curvature of the IEAP can be calculated from dip displacement δ as follows:

$$\kappa = \frac{2\delta}{l^2 + \delta^2} \tag{5.2}$$

Figure 5.4 shows that despite the relationship (5.2) being a power function, in the range of experiment-driven values (κ = –100–100 m^{-1}), the correlation between curvature and tip displacement can be approximated to linear.

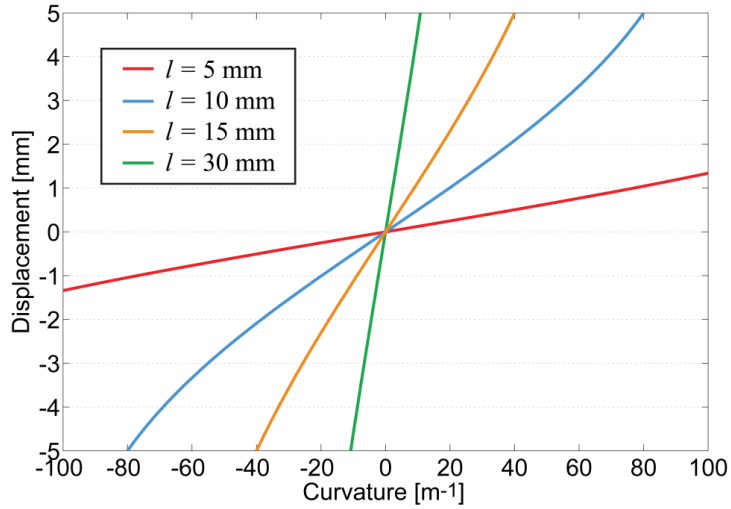

Figure 5.4. Correlation between the displacement and the curvature of an IEAP actuator.

The best fit for experimental data in figures 3.8(a) and 3.10(a) is an exponential function in the form of:

$$R(\kappa) = Ae^{B\kappa} + C \tag{5.3}$$

A, B, and C are correlation coefficients related to electrode material and dimensions of the IEAP sample. For the IPMC sample characterised in chapter 3, one suitable set of correlation coefficients is:

$$\begin{cases} A = 1.439 \\ B = -0.035 \\ C = 5.371 \end{cases}$$

Bridge output (supply voltage of 1 V) is described by the following equation:

$$V_{BRIDGE} = \frac{R(-\kappa)}{R + R(-\kappa)} - \frac{R(\kappa)}{R + R(\kappa)} \tag{5.4}$$

By calculating output of the bridge based on equations (5.3) and (5.4) with empirical coefficients A, B, and C, figure 5.5. is obtained.

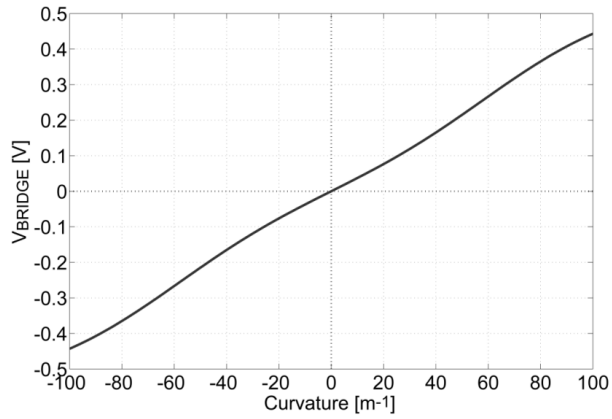

Figure 5.5. Simulated output of bridge circuit when resistance is changing exponentially on both legs.

In conclusion, regarding the dimensions of typical IEAPs, conversion between curvature and tip displacement can be considered relatively straightforward as it is feasible to utilise linear approximation. Furthermore, in the case of exponential change in electrode resistance due to alteration of curvature, bridge output voltage correlation to curvature (or tip displacement) can be regarded linear, thus lessening the complexity of the proposed self-sensing system.

5.4. Manufacturing techniques

In this section three different methods for patterning are described and compared in detail:

1) manual scraping;
2) machining;
3) laser ablation.

The first approach to obtain the described pattern was by using a sharp blade to manually scrape the necessary grooves in the platinum electrodes. Even though this method is sufficient for separating the different sections of the device, it is unwieldy, time-consuming and the accuracy is low.

As a second method for patterning a Wabeco CC-F1410 LF high speed CNC milling machine with a Ø0.8 mm hard metal end bit was adopted. The IPMC sample was moved at the velocity of 2 $mm \cdot s^{-1}$ and the spindle speed was set to ~3750 rpm. This method has several characteristic disadvantages and requires training and skill. Due to the softness of IPMC, its surface is uneven under the

mill. Since the thickness of the metal electrodes of the IPMC is ~10 μm, several IPMCs were damaged before obtaining the necessary skills. In the end some of the polymer membrane was still cut during the process of removing the platinum. This, however, was not a major concern, as the integrity of the Nafion beyond the actuator section is only necessary for the purpose of keeping the whole device in one piece. Therefore, removal of the polymer membrane within reasonable limits is acceptable as long as the IPMC device stays intact. Another difficult task was to position the sample properly after turning it over in order to remove the metal from exactly the same place on both surfaces. The dimensions of patterns achieved by machining are limited by the diameter of the mill bit. Despite the inconveniences, several IPMC sheets were patterned successfully.

The third approach for producing the patterns was to evaporate the metal electrode by implementing a pulsed UV excimer laser. A KrF excimer laser (Coherent COMPex Pro 205F, wavelength 248 nm, pulse duration 25 ns) was used for the ablation. The laser beam was focused on the IPMC sheet by fused quartz lenses. The optimal laser pulse energy and repetition rate were acquired by trial and error. For platinum-coated IPMC with a Nafion polymer membrane, the most appropriate configuration was with a pulse energy of 12–13 mJ. The frequency of the laser pulse used was set to 10 Hz and during patterning the IPMC was moved at a constant speed of 0.1 $mm \cdot s^{-1}$ with the help of a CNC bench.

Nafion is virtually transparent in the UV/vis spectrum [90] and therefore it is possible to evaporate metal simultaneously from both sides of the IPMC. Since very little of the laser's energy is absorbed in the Nafion, only the approximately 10 μm thick platinum electrode is vaporised. The first pulse removes metal from the top face of the IPMC material, the next pulse aimed at exactly the same spot removes metal from the opposite face. By pointing the laser beam onto just one surface, it is feasible to create concurrently similar patterns on both sides of the IPMC without causing any mechanical damage to the polymer membrane. This eliminates the need to turn the sample around for realisation of patterns on both surfaces as is required for machining.

It is theorised that elimination of platinum is a result of three concurrent mechanisms occurring at considerably different temperatures: vaporising of the platinum, melting of the Nafion, and boiling of the solvent (*i.e.* water). Therefore the parameters of the laser impulses need to be a careful optimisation between a low duty cycle and relatively high energy levels to achieve effective patterning.

Figure 5.6 shows the IPMC samples fabricated using the three methods described above. Evidently it is most impractical to scratch off the platinum electrodes manually. The greatest disadvantages of machining are the constraints on mill size and the unevenness of the IPMC samples. It was difficult to find a mill bit smaller than Ø0.8 mm that could resist the strength of the platinum. As expected, laser ablation proved to be the most suitable method for this kind of patterning. The most significant advantage of using a laser is the possibility of simultaneously removing metal from both sides of the sample

without harming the polymer membrane. In addition, laser ablation can provide better precision and finer patterns than machining or manual scraping. Also, out of the three methods described in this section, laser ablation is best suited when patterning IPMC with relatively thin polymer membranes as the laser only removes electrode material and leaves Nafion intact.

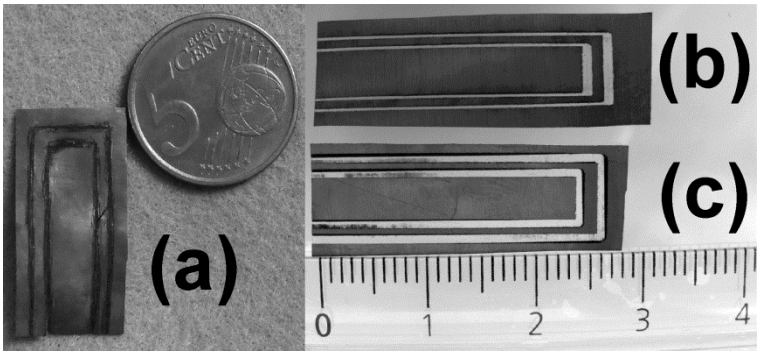

Figure 5.6. Patterns achieved by (a) manual cutting using a sharp blade, (b) laser ablation, and (c) machining. A ruler in (b) and (c) is provided in centimetre scale.

5.5. Qualitative analysis of patterning

Methods of laser ablation and machining heat the processed substances up. It must be pointed out that laser cutting of metal electrodes from wet ionic polymer is a controversial procedure: the polymer should vanish long before the metal because the melting point of platinum is 1768 °C but the decomposition temperature for ionic polymers lies in the range of just 200–300 °C. Surprisingly the laser ablation does not destroy the polymer membrane although its decomposition temperature is an order of magnitude lower than the melting point of platinum. In order to investigate the produced patterns and the effects of patterning (especially the influence of laser ablation) on the polymer membrane, three different methods of characterisation were used: optical microscopy, electrochemical impedance spectroscopy, and Fourier transform infrared (FTIR) spectroscopy.

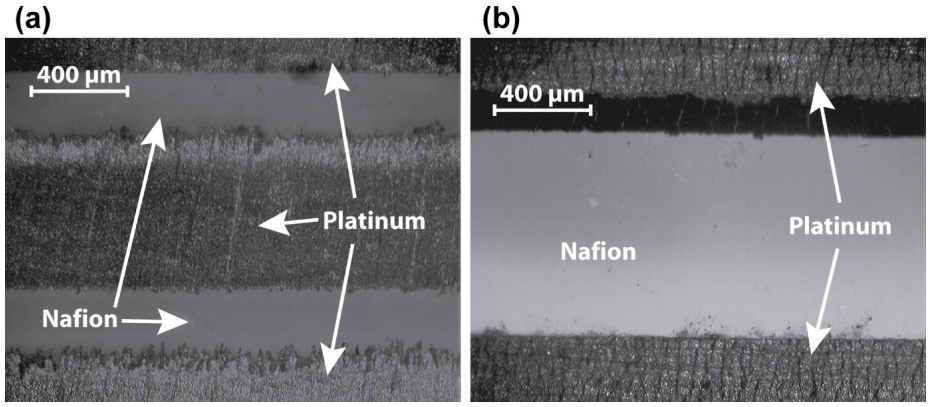

Figure 5.7. Optical microscope pictures of patterns created by a) laser ablation and b) machining.

Figure 5.7 depicts microscope pictures of patterns created using laser ablation and machining respectively. Besides the fact that the widths of the patterns are different, it is clearly visible that laser ablation detaches platinum by shreds, leaving a rather jagged edge. It is likely that there are two concurrent mechanisms of platinum removal: heating of the platinum until evaporation; but mostly the steam of the boiling water explodes and throws the shreds of platinum off. Therefore, the removal of platinum can be regarded as a form of material-assisted laser ablation (MALA) [91] where the assistant agent is water from the IPMC. However, machining proves to create a very smooth cut. The distinctive dark area right under the platinum electrode in figure 5.7(b) illustrates the issue of not always achieving concurrent patterns via machining, since it is actually the platinum electrode on the other face of the sample. Due to the previously mentioned feature of simultaneously patterning both electrodes, such problems are not present in laser ablated samples of IPMC (figure 5.7(a)).

The second approach, electrochemical impedance spectroscopy, was conducted using the potentiostat PARSTAT 2273 from Princeton Applied Research. The impedance between two different sections (e.g. sensor and shielding electrode) on the same side of the IPMC was measured in the frequency range of 10 mHz–10 kHz at a V_{RMS} of 40 mV.

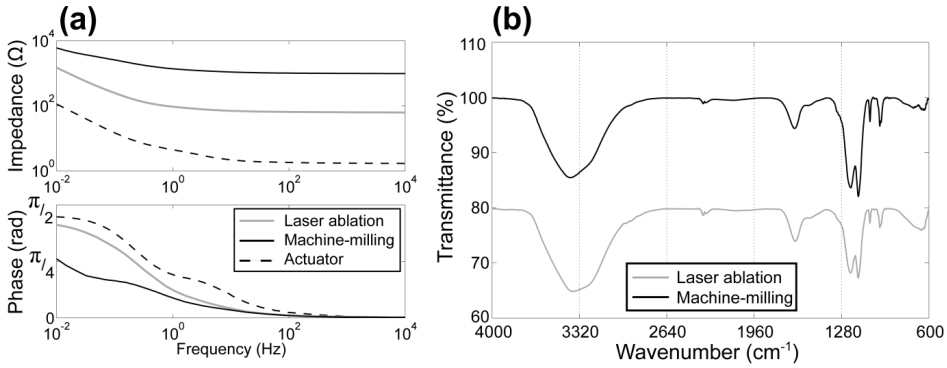

Figure 5.8. a) Bode plot of the machined and laser ablated patterns and the whole IPMC actuator. b) FTIR spectra of the Nafion from the patterned samples. The laser ablation curve has been shifted by −20 along the *y*-axis for better readability of the graph.

The Bode plot of the measured impedances is given in figure 5.8(a). The highest magnitudes of impedances are attained on the machined IPMC sample, which can be explained by the width of the cut on the electrode. The groove in the platinum left after machining is approximately 1 mm, while laser ablation produces only a 300 µm wide cut. As a reference, the cross-electrode impedance of the whole actuator (*i.e.* from one electrode to the other) is also given. As expected, it demonstrates the smallest impedance values because the thickness of polymer between the electrodes is roughly 200 µm.

In order to investigate whether the laser ablation changes the chemical structure of the Nafion and incidentally influences the performance of the whole device, FTIR spectroscopy was utilised.

To acquire Fourier transform infrared spectra of the Nafion from under the removed platinum, a PerkinElmer Spectrum BX FTIR spectrometer with a ZnSe crystal from Interspectrum Ltd (Estonia) was implemented. This apparatus allows measurements of the Nafion without removing it from the rest of the IPMC – the IR beam was simply pointed on the polymer part of the self-sensing actuating device. Spectra were collected as an average of 16 scans with a resolution of 2 cm^{-1} in the range of 4000–600 cm^{-1}.

The FTIR spectra given in figure 5.8(b) demonstrate that the Nafion from the laser ablated IPMC follows the same behaviour as that from the machined sample. These results comply with earlier research in the field of Nafion FTIR spectroscopy [92,93]. It must be noted that the drop of transmittance at approximately 3400 cm^{-1} is solely due to the water inside the polymer membrane while the behaviour of the transmittance at 1230–1140 cm^{-1} is typical for Nafion. These spectra indicate that the laser ablation really removes only the platinum and does not cause any harm to the Nafion. This again implies that the only process responsible for casting off the platinum during laser ablation is the pressure from the steam of the boiling water.

These results demonstrate that none of the patterning methods alter the electrochemical properties of the gaps between the separate electrodes or affect the actuating performance of IPMC. In spite of their convenience levels for the production, all the described techniques are applicable for manufacturing similar patterned IPMC devices. The choice of method should be argued solely on the cutting precision and cost.

5.6. Experimental

This section describes setup for experiments conducted with patterned IPMC samples (figure 5.9).

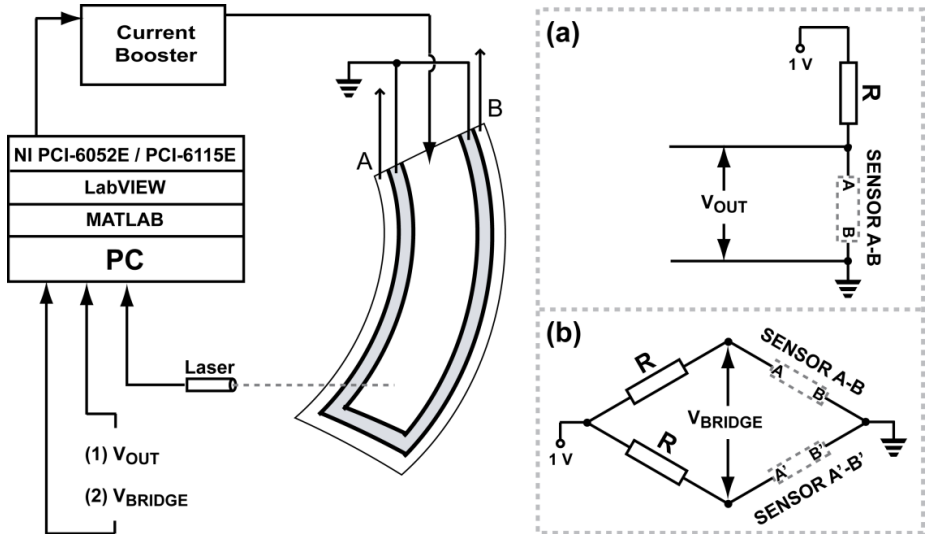

Figure 5.9. Experimental setup.

The proof-of-concept experiments were mainly carried out on an IPMC with manually scraped patterning. The input signal of the actuator was a low-frequency sine wave (f = 0.5 Hz), with peak-to-peak voltage of 4 V. The sinusoidal input was chosen in order to avoid any high-frequency cross-talk between the actuator and sensor electrodes. As this IPMC strip exhibited relatively high cross-talk between the actuating and sensing elements, the sensor electrodes of the opposite sides of the IPMC were connected in a bridge configuration (figure 5.9(b)). Assuming that the cross-talk is similar on both sides (*i.e.* it represents the common mode noise), the bridge circuit cancels out the undesired signals. In order to further suppress any cross-talk, the shielding electrode (figure 5.1) was connected to the system ground.

In the course of the proof-of-concept experiments, the IPMC strip was held fixed between a stationary clamp for approximately 8 s while the actuating signal was applied to it. After this period elapsed the IPMC was released and was free to bend. Such a procedure allowed determination of whether the acquired signal was caused by the movement of the IPMC actuator or was the undesired effect of cross-talk. If the sensing signal is produced only when the IPMC bends, it can be argued that the results obtained are not caused by conductive and/or capacitive coupling.

Patterning methods such as laser ablation and machining provide rather good insulation between the actuator and the sensor element; hence, there is no systematic error present on the sensor electrode that would require a differential measurement scheme. Therefore a simple voltage divider was sufficient for determining change of resistance between terminals A–B (figure 5.9(a)).

The displacement of the IPMC strip during the actuator's working cycle was measured using a laser displacement sensor. In proof-of-concept measurements, the laser sensor was pointed at the actuator at roughly 14 mm from the clamp holding the IPMC in a cantilever configuration. The actual displacement of the tip of the actuator-sensor system was larger than visible on graphs (figures 5.10–5.12). However, when validating the new electromechanical model, the laser displacement sensor was pointed at the tip of the actuator segment of the IPMC sample.

The experiments were conducted with two types of IPMCs. First IPMC material was prepared in-house: it consists of Nafion 117 as polymer with different cations, and platinum as metal electrodes. Although it is a water-containing IPMC, it works in air even after partial drying. The experiments with this material were conducted in air conditions. The second IPMC material was Musclesheet IPMC provided by Biomimetics Inc. It is a water-containing proprietary ionic polymer membrane with Na^+ cations and platinum as electrodes. This material was used exclusively in deionised water.

5.7. The proof of concept

The proof of concept for proposed self-sensing system was conducted on an IPMC with manually scraped patterning.

Figure 5.10 gives the typical outputs of the bridge circuit and the corresponding laser position sensor. While the IPMC strip is held fixed, no significant signals are produced by both the bridge and the laser position sensor. After releasing the IPMC at t_{rel}, a relevant signal can be observed upon the bridge. Figure 5.10 shows that the signals produced by the two motion measurement systems are strongly correlated. IPMC strip is forced out of its natural shape, while fixed between the clamps, thus there is a sharp flexion of IPMC when it is released from the hold. For both motion sensor systems, this process can be observed as the rapid change of offset levels at t_{rel} in figure 5.10.

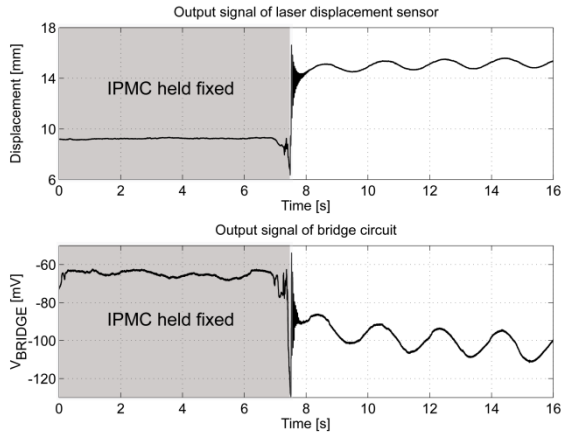

Figure 5.10. Typical outputs of the bridge (V_{BRIDGE}) and the laser displacement sensor.

Data prior to time t_{rel} was discarded in order to gain relevant information about the displacement from the electrode sensor output of the IPMC strip. Also a trend due to the dehydration of IPMC has been removed from the signals of both laser sensor and bridge. Figure 5.11 presents the outputs of the resistive sensor electrode and the laser sensor after these manipulations.

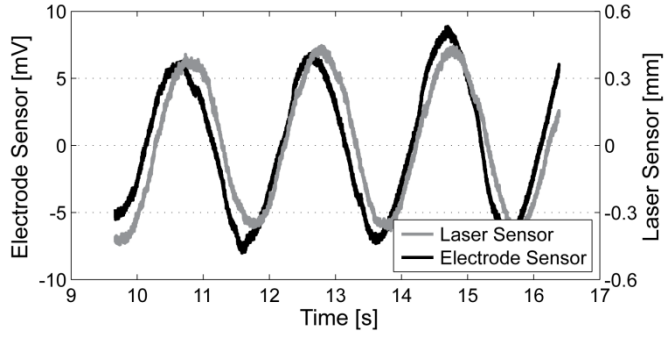

Figure 5.11. Electrode and laser sensor outputs.

The scatter plot of the laser and electrode sensors is visible in figure 5.12. It can be clearly seen that the relationship is nearly linear in the investigated deformation range with the coefficient of determination $R^2 = 0.8243$. When the displacement increases (*i.e.* the IPMC moves away from the laser) the bridge output signal also rises.

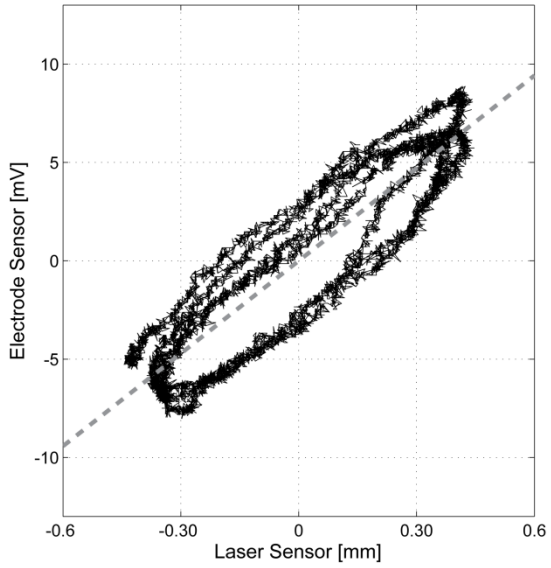

Figure 5.12. Correlation between laser sensor and IPMC electrode sensor output data.

The slight discrepancy between the two signals can be caused by the fact that electrode resistance changes differently on compression and expansion (chapter 3). So the bridge circuit is not completely balanced and this might be the cause for the loop-like scatter, observed in figure 5.12.

In order to investigate the range of the low frequency input voltages of the actuator, in the next experiment, a sine sweep test signal was used to actuate IPMC. As expected, at higher frequencies the cross-talk increases significantly. Regardless, the IPMCs are commonly intended to be used for low frequency (less than 2 Hz) values of the input voltage due to the large power consumption observed at higher frequencies [69]. It can be expected that by varying the width of patterns, it is possible to make the system viable at higher frequencies.

More specifically, the results of the sweep test in the frequency range of 1 mHz to 1 Hz are given in figure 5.13. The duration of sweep signal was 10 s and the experiment lasted for 50 s. During the first 16–17 s the IPMC was fixed between stationary clamps. The graphs depicted in figure 5.13 show that while the IPMC is held still, there is no sensing signal from the electrode, but when it can bend freely, the changes in the output of the bridge become evident. This affirms that the acquired signal is generated due to the deformation of the IPMC and not because of the cross-talk.

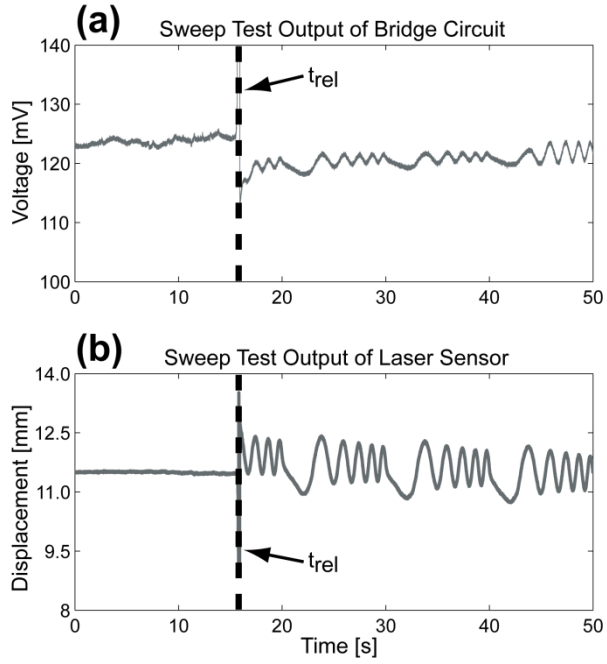

Figure 5.13. Frequency sweep test. a) Bridge signal; b) Laser displacement sensor signal.

Figure 5.14 depicts a series of experiments conducted on IPMC strips patterned by means of laser ablation and machining. In these experiments actuation is externally blocked for 4 s and sensing signal from one electrode layer is obtained by means of a voltage divider.

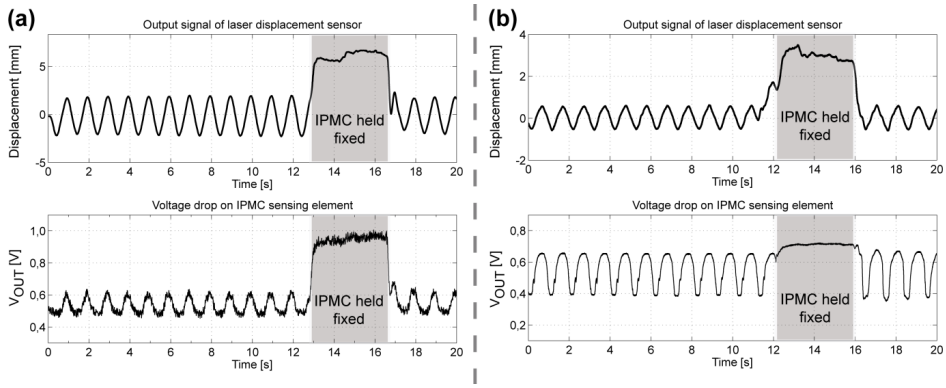

Figure 5.14. Laser displacement sensor and sensing signals acquired from self-sensing IPMC with patterns created by a) machining, b) laser ablation.

5.8. Electromechanical model

In the current section a straightforward model of the patterned self-sensing actuator is proposed. The model will link the sensor electrode resistance variation with the tip deflection of the actuator.

In the interest of simplicity and usability the following few assumptions were made:

1) The electrode material has only resistive behaviour;
2) The IPMC beam undergoes pure bending;
3) The beam is homogeneous.

Despite IPMC consisting of different layers, in this model the device is considered homogeneous having uniform rigidity. The Young's modulus E of the whole device can be regarded as $\int \epsilon(y)dy$, where $\epsilon(y)$ is the Young's modulus as a function of the location along the thickness t of the device (figure 5.15).

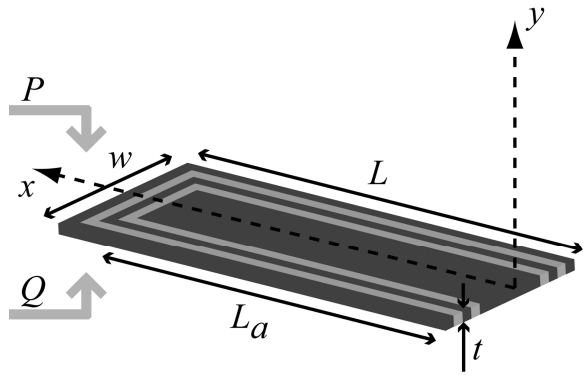

Figure 5.15. Geometry of the self-sensing IPMC device.

The Euler–Bernoulli theory of beams is based on the assumption that a relationship between bending moment and beam curvature is mathematically stated as

$$\kappa = \frac{M}{EI} \tag{5.5}$$

where κ, M and EI denote the beam curvature, the bending moment at any cross-section of the beam, and the bending rigidity of the beam, respectively. Further it can be claimed that

$$\frac{\Delta L}{L} = \frac{t}{2}\,\kappa \tag{5.6}$$

where ΔL is the change in length of the beam's surface, *i.e.* at the distance of half-thickness – $\frac{t}{2}$ – from the neutral axis.

The tip displacement d of a beam is described by following formula

$$d = \frac{M}{2EI} {L_a}^2 \tag{5.7}$$

By combining (5.5), (5.6) and (5.7), it is obtained that the correlation between the change of lengths of the opposite electrodes P and Q of the device, and the tip displacement is described by

$$\Delta L_P = \frac{tL}{{L_a}^2} d \text{ and } \Delta L_Q = \frac{tL}{{L_a}^2} d \tag{5.8}$$

The proposed patterned system can be interpreted as a strain gauge described by a gauge factor G.

$$\frac{\Delta R}{R_S} = G \frac{2\Delta L}{L_S} \tag{5.9}$$

R_S and L_S are correspondingly the initial resistance and length of sensor element. Due to the geometry of the proposed IPMC sensor (figure 5.15), ΔL has to be multiplied by 2 as presented in (5.9), and the sensor length L_S is

$$L_S = 2L + w \tag{5.10}$$

Equation (5.8) in combination with (5.9) presents means for experimentally evaluating the gauge factor G required for the current electromechanical model.

After experimentally evaluating the gauge factor G for the IPMC electrode, it is possible to predict the resistance variation along the sensing element of the patterned sample.

At last, equations describing the relation between the resistance change of the electrodes and tip deflection are expressed. By combining (5.8) and (5.9) it is obtained that:

$$\frac{\Delta R_P}{R_{SP}} = G_P \frac{2tL}{{L_a}^2 L_S} d \text{ and } \frac{\Delta R_Q}{R_{SQ}} = -G_Q \frac{2tL}{{L_a}^2 L_S} d \tag{5.11}$$

The gauge factors G_P and G_Q are different for the opposite electrodes of the device, depending on the type of deformation and on the initial resistance of the electrode. In chapter 3 and the paper by Punning *et al.* it is established that when the electrode is compressed, its resistance decreases slightly but when the electrode is stretched, the increase of resistance is much more considerable [51]. Therefore, in case of equal initial resistances, the absolute value of gauge factor for a compressed face is smaller than the one for the electrode undergoing stretching.

Experiments for validating the model were conducted as follows:

1) a sinusoidal actuating signal (V_{PP} = 3 V, f = 1 Hz) was applied to the actuator part of the IPMC sample;
2) a sensing signal (V_{OUT}) was measured (at the rate of 100 samples·s^{-1}) from the sensor element of the self-sensing device;
3) a Banner LG10A65PU laser displacement sensor (calibrated for underwater measurements) was used to determine the actual tip displacement of the actuator part;
4) the gauge factor G was evaluated from one work-cycle of the actuator by using equation (5.11);
5) further measurements were conducted using this gauge factor G.

The parameters required to estimate the tip displacement from the resistance change of the single sensor element are provided in table 5.1. In the presented experiments the gauge factor was found experimentally during one work-cycle (one period of input signal) of the actuator. Equation (5.8) provides the relationship between the change of electrode length and the tip displacement during the measurements. Combining equations (5.9) and (5.8) gives the behaviour of G during the actuator's work-cycle. In the course of this experiment, the gauge factor remained constant within the implemented range of accuracy. Since the simulation data are calculated from the change of resistance, a smoothing of the measured resistance values was conducted using a method of moving average over 16 samples. After experimentally evaluating the gauge factor G, the simulation curve was calculated using equation (5.11).

Table 5.1. Values used for simulating the tip displacement.

Symbol	Value
G	395
R_S	311 Ω
L_a	0.024 m
L	0.027 m
L_S	0.064 m
t	0.0002 m

The experimental validation of the proposed electromechanical model is given in figure 5.16, featuring the simulated and measured tip displacements of the IPMC actuator. The simulation curve follows the experimental data relatively well, though there is a slight discrepancy during the negative half-period. This is caused by the fact that the electrode resistance changes differently on compression and stretching. This could be overcome by implementing the gauge factor as a function or by measuring the sensor signal from both electrodes of the device.

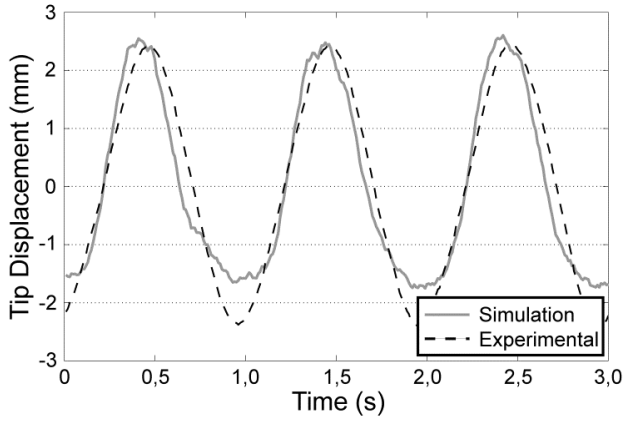

Figure 5.16. Comparison of the measured and simulated tip displacements of the self-sensing IPMC actuator device.

5.9. Conclusions

In this chapter a self-sensing ionic polymer-metal composite was developed by means of patterning different segments for sensing and actuation on a single piece of IPMC. Alteration of electrode resistance due to IPMC bending was chosen as the feedback mechanism for this system. In order to suppress undesired cross-talk from actuator to sensor, an intermediate shielding electrode that is connected to the system ground is patterned between sensing and actuating elements.

Patterning of the electrodes was achieved by three different techniques: manual scraping, machining, and laser ablation. Detailed description of the patterning processes with qualitative analysis was given.

Experimental proof was given on the feasibility of self-sensing IPMC with patterned electrode layers. Eventually a straightforward model for such device was proposed and validated.

6. SELF-SENSING IONIC ACTUATING DEVICE WITH PATTERNED CARBON ELECTRODES

6.1. Introduction

According to chapter 3 and paper I of this thesis, resistance of electrode layers of carbon-polymer actuators can also be exploited for curvature and position sensing. Therefore implementing a design of a previously proposed self-sensing device (chapter 5) with patterned electrode on CPC actuators is also justified. However, the compositional variances and dimensional differences in layers of different IEAP make it difficult to directly transfer the methods of IPMC patterning to CPC electrodes.

While feasible, machining a CPC electrode is challenging as the polymer backbone that would be responsible for holding the patterned system together is 20–30 μm thick while a single electrode thickness is 6 times that – 150 μm. During machining the polymer backbone can easily be harmed as the electrode material would need to be removed in the full depth of its thickness to minimise conductive coupling between different sections of an electrode. Hence, the resolution of a CNC becomes a critical factor.

Carbon patterning is well-studied for application in MEMS where dimensions of the material are an order of magnitude smaller than in CPCs. Most often used methods for patterning carbon films include direct laser ablation [94], plasma etching [95], and controlled growth of carbon film on pre-patterned surface [96]. However, all these methods can be considered unsuitable for patterning carbon-polymer composite electrodes. Pulse energies required for direct laser ablation of carbon particles would most likely destroy the polymer membrane [94,97]. In spite of the less destructive alternative, called the material-assisted laser ablation, the pulse energies remain high enough to potentially damage the polymer backbone [91]. Moreover, the extremely high voltage of plasma etching could also supposedly harm the integrity of ionic liquid and the controlled growth of carbon nanotubes takes place at relatively high temperatures which leads to the melting of the polymer membrane. Therefore, all the above mentioned patterning techniques can be considered risky for CPC actuators.

Nevertheless, printing of customised carbon electrodes would be a feasible option for creating necessary patterning for a CPC actuator [98] as it does not involve cutting, heating or high electric field that could possibly damage separator polymer or ionic liquid.

This chapter proposes a method for patterning carbon electrodes of a CPC by means of spray painting the electrodes on a previously masked membrane. After removing the mask, a self-sensing multi-segmented carbon-polymer actuator is attained. While the relatively low conductivity of such electrodes proved to be a hindrance on actuation, the proof of concept for such a self-sensing CPC actuator is demonstrated.

6.2. Patterning carbon electrodes

A membrane consisting of PVdF(HFP) and ionic liquid was masked by a tape as shown in figure 6.1(a). A solution with carbon particles was then painted on this membrane. Masking tape was carefully removed and the sample was cut into the appropriate shape, thus, patterned electrodes were achieved (figure 6.1(b,c)).

The separator membrane was prepared from an $EMIMBF_4$ and PVdF(HFP) solution (1/1 wt). The IL was added to the polymer solution (4-methyl-2-pentanone and propylene carbonate were used as solvents), sonicated for 25 min, and then poured into a polytetrafluoroethylene (PTFE) mould.

The solution of electrode paint was made of PVdF(HFP), $EMIMBF_4$, CDC, SWCNT (33/36/30/1 wt) and dimethylacetamide (DMAc) was used as solvent. SWCNTs were used to increase the conductivity of the electrode [99]. First step was dissolving PVdF(HFP) in DMAc. The mixture of millimetre long SWCNTs and DMAc was measured into another vial and treated with an ultrasonic probe to unbundle SWCNTs. Next, $EMIMBF_4$ and titanium carbide-derived carbon were added to the solution of the unbundled SWCNTs and treated with the ultrasonic probe. Finally, the polymer solution was added and treated more with the ultrasonic probe.

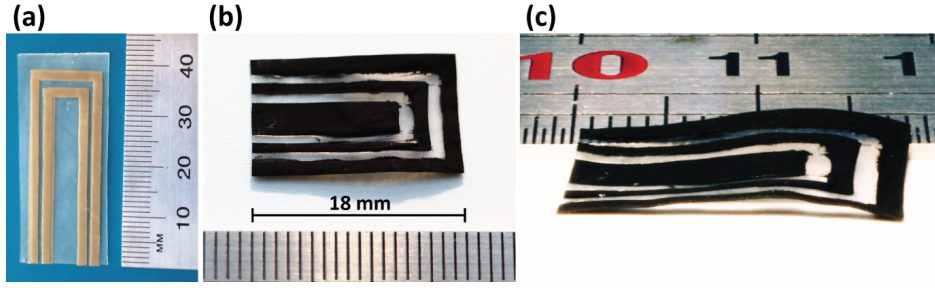

Figure 6.1. a) PVdF(HFP) film after masking it with brown tape. b), c) CPC actuator with patterned electrodes.

Separator membrane was masked by adhesive tape (figure 6.1(a)). Requirements for masking tape include good adhesion to separator during painting procedure as the solvent from electrode paint causes the membrane to soften and start curling. Plus, the tape and its adhesive must not dissolve in DMAc – the solvent for the electrode paint. Several tapes were tested and a brown packing tape (Vibac) met all the required criteria.

Electrodes were applied directly to the masked membrane by spray painting 15 layers on each side. Hot air was used to expedite the drying of paint before the next layer was applied. Finally, the tape was carefully removed and the

sample was cut into appropriate size and shape, yielding a patterned CPC actuator depicted in figure 6.1(b,c).

6.3. Qualitative analysis of created pattern

There are some key aspects to patterning that need to be considered after the patterns are created on IEAP electrodes:

1) Is the outcome of patterning as expected?
2) Is the insulation between the sections for actuator and sensor sufficient to suppress cross-talk that could interfere with the sensing signal?

In figure 6.1(b,c) it is depicted that as a result of the patterning, clearly separated sections for actuation, shielding, and sensing are obtained. While optical microscope images (figure 6.2) confirm the success of patterning, it is also apparent that when the adhesion between the masking tape and the polymer membrane fails, the electrode solution can flow under the mask (see top right in figure 6.2(a)).

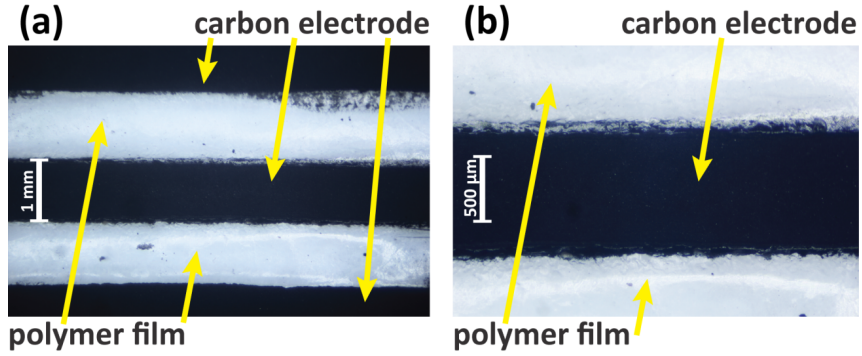

Figure 6.2. Optical microscope pictures of created patterns.

EIS measurements were carried out with PARSTAT 2273 in the frequency range of 10 mHz to 10 kHz at V_{RMS} = 40 mV. Two kinds of impedances were acquired – measured from one section to another (e.g. between the actuator and the shielding, denoted as *pattern* in figure 6.3) and cross-electrode measurements of the actuator section (denoted as *actuator* in figure 6.3).

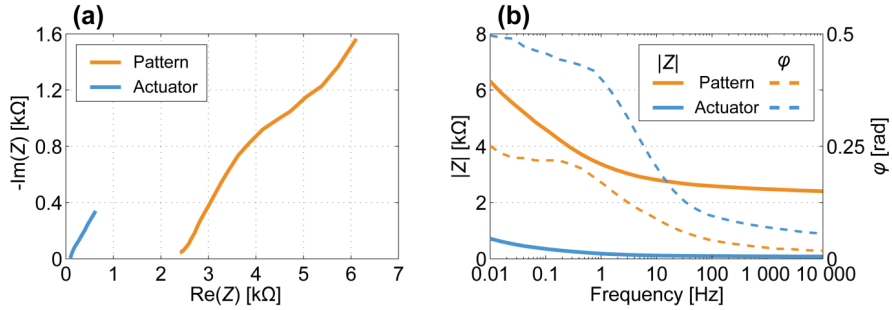

Figure 6.3. Nyquist and bode plots for impedances between two sections of electrode layer (pattern) and opposite electrodes of an actuator section.

From the impedance data it can be concluded that the magnitude of impedance from one segment to another is several times higher than from one side of the actuator to another. However, while different in scale, the shapes of these curves in figure 6.3 are very similar, thus, suggesting that a weak actuator is created between different segments of the electrode layer. While this may prove to be important for understanding what type of mechanism is responsible for noise and signal propagation (e.g. similar transmission line models could be adopted for actuator as well as for cross-talk), the actual electromechanical effect between patterned sections can be considered negligible.

Next, a study of signal propagation between different segments was carried out. A driving signal was applied to the actuator segment and voltage drop on sensor segment of each electrode layer was acquired. The response from the sensing section was determined to be symmetrical on both sides of the device and the effect of noise reduction with grounding the shielding electrode is demonstrated in figure 6.4. As the driving signal is propagated to the sensor section, the grounded shielding electrode lessens this undesired noise by roughly a factor of two. However, in current prototypes, the cross-talk from actuator to sensor could not be fully suppressed.

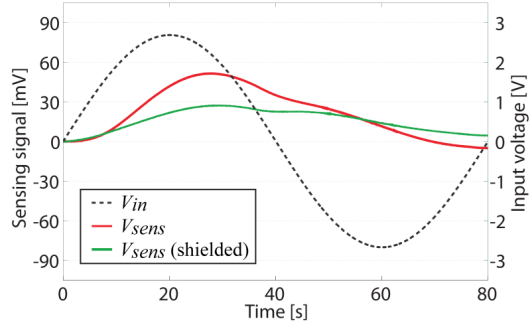

Figure 6.4. Input signal and voltage drop on sensing segment with and without the shielding electrode connected to the system ground.

6.4. Experimental

An experimental setup similar to the one described in section 5.6 was adopted. As the cross-talk from the actuator to the sensing section could not be fully supressed (figure 6.4), a bridge configuration was chosen to measure the sensory signal. Bridge with supply voltage of 1 V was balanced with two external resistors of 1.2 kΩ.

The sample was positioned in a cantilever configuration and for signal generation as well as acquisition, a PC with NI PCI-6036E DAQ card and LabVIEW was utilised. Sinusoidal driving signal V_{in} (2.7 V, f = 12.5 mHz) was generated at the sampling frequency of 100 Hz, while data acquisition rate was chosen to be 500 samples·s^{-1}. Laser displacement sensor Keyence LK-G82 in combination with multifunctional controller LK-G3001P was used to measure tip displacement, the laser spot was aimed at the far end of actuator segment, *i.e.* approximately 10 mm from the fixing clamp.

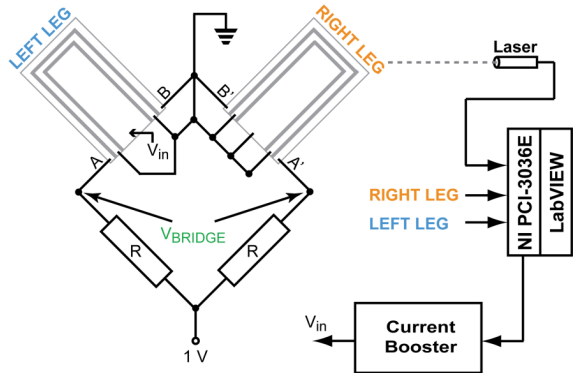

Figure 6.5. Experimental setup.

A sensing signal was acquired on both sensing electrodes (left and right leg of the bridge, figure 6.5) and the calculated difference of these signals is denoted as V_{BRIDGE}. For characterisation of pure sensing capabilities of the sensor segment, the actuator driving signal was set to 0 V and bridge output in response to external manipulation of the sample was acquired.

As the overall amplitude of actuation remained relatively small, external manipulations of the actuator were used to demonstrate the self-sensing capabilities of the proposed system.

6.5. Results

Figure 6.6 depicts the input signal, current, and tip displacement of the CPC actuator with patterned electrode layers.

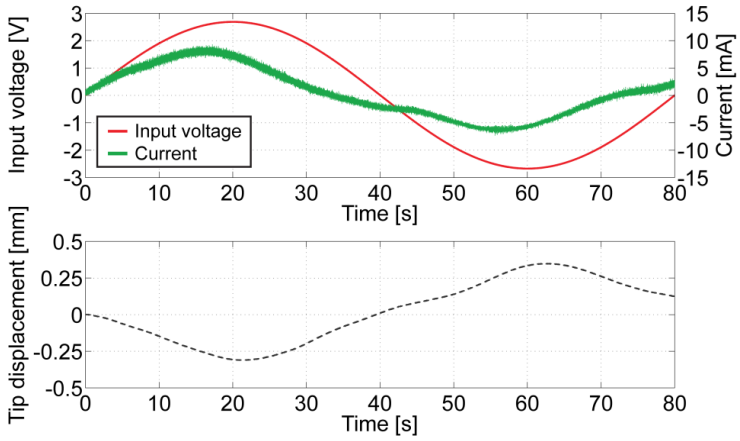

Figure 6.6. Electromechanical properties of created actuator.

In order to investigate sensing capabilities of the sensor sections of the electrodes, the CPC sample was manually assisted. Figure 6.7(a) shows that synchronously with bending of the device a signal is measured from the bridge. Figure 6.7(b–d) depicts the relation between the tip displacement and different signals measured from the bridge circuit.

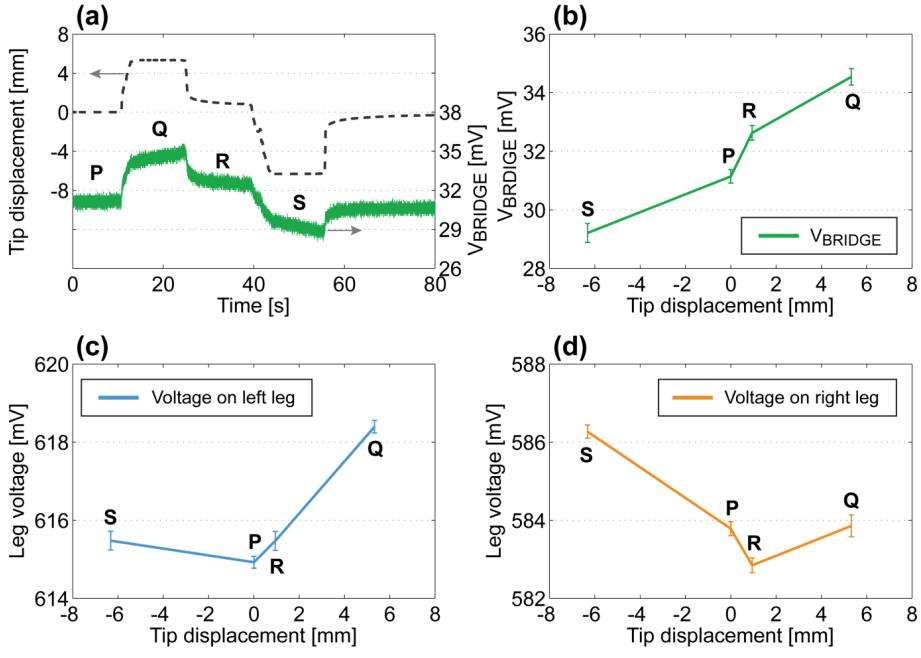

Figure 6.7. Sensing capabilities of sensing electrode.

When external manipulation was introduced during the work-cycle of the self-sensing CPC device, a distinct sensorial effect is registered from the bridge circuit (figure 6.8). Figure 6.8 displays two different cases of external manipulations affecting actuator displacement. Both bidirectional (figure 6.8(a,c)) rapid dislocations of the actuator as well as slower unidirectional (figure 6.8(b,d)) bending are registered from the sensing electrode.

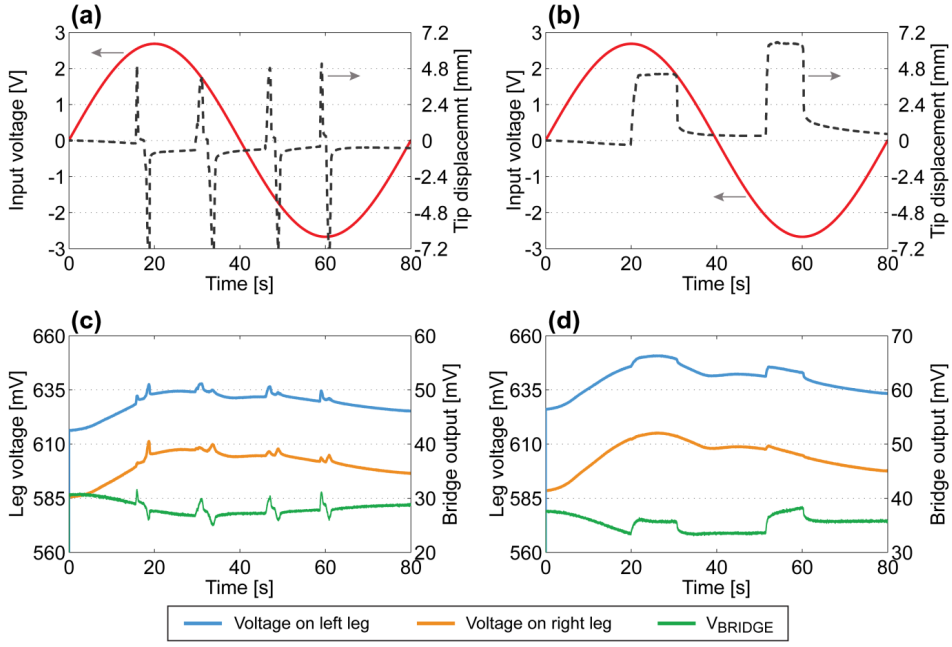

Figure 6.8. Self-sensing capabilities of CPC actuator.

6.6. Discussion and conclusions

Based on the reported results, the proposed method of spray painting carbon electrodes on a solid polymer membrane is feasible for creating working EAP actuators with patterned electrodes. It was shown that such cIEAP is able to actuate and its electrodes present a sensing effect based on the change in resistance.

The proof of concept for the self-sensing IEAP actuating device with patterned carbon electrodes was presented. However, several issues yet remain open. In the developed prototypes, as the overall amplitude of actuation was too small to clearly surpass the issues related to the electrical noise, the self-sensing ability was demonstrated with the manual obstruction and assistance of the device. Noteworthy sensing signals were registered when curvatures, larger in scale compared to electrically-induced bending were applied to the working

prototype. The experiments affirm that the device of better actuation performance is capable for sensing its own deflection without external assistance.

There are two factors constraining the actuation of the created system: low electrode conductivity of the actuator section and large passive area of the device (*i.e.* non-actuating segments such as shielding and sensing electrodes, plus the area between them). As only the actuator section is responsible for bending the whole device, it is critical to optimise the complete device for actuation. With present conductivity of electrodes, the actuator is exhibiting a relatively small amplitude which is mainly induced by bending occurring near the fixing clamp of the actuator. It is possible to enhance the actuation performance by increasing the conductivity of the electrode by varying the composition of electrode paint or adding an extra layer of metal to the actuator section. Moreover, mostly due to unwieldiness of the preparation process, for existing prototypes the area of actuator section is merely 24% of the area of the whole self-sensing device. By adopting machine-assisted methods (such as inkjet printing) the area of passive sections can be reduced down to limitations set by wiring and cross-talk.

The resolution of sensing was decreased due to the electrical coupling between the actuator and the sensing elements, *i.e.* the cross-talk. While the grounded shielding electrode considerably reduces the amplitude of cross-talk (figure 6.4), it still fails to suppress it completely. As visual inspection of the patterns revealed no carbon-based conductive paths between different sections of the electrode layer, the residual cross-talk was presumably due to the relatively small conductivity of the shielding electrode. The shielding electrodes made of metal or some other rather conductive material would decrease the effect of electrical coupling similarly to the patterned IEAPs with platinum electrodes.

In some cases the change in resistance of the carbon electrodes of particular CPC materials is not dependent on the direction of the bending [75,100]. While the magnitude of this change differs considerably on electrode compression and expansion, the overall direction of bending can only be attained by comparing the resistance change on both sides. Here the bridge circuit, initially intended for suppressing common mode noise related to cross-talk, provides supplementary information on the bending direction.

7. CONCLUSIONS

This thesis compiles together the work towards a self-sensing ionic electro-mechanically active polymer actuator. IEAPs with two distinct types of electrode material – carbon and metal – are studied and self-sensing devices with patterned electrode layers are designed, produced and modelled.

The underlying principle for the self-sensing devices developed is the alteration of electrode impedance in response to material curvature. Chapter 3 presents an extensive study of electrochemical impedance spectroscopy of two distinct IEAP materials (IPMC and CPC) resulting with two significant conclusions:

- Impedance measured from electrode layer of IPMC and CPC is strongly correlated to material curvature.
- A transmission line electrical equivalent circuit for CPC was proposed where electrode layer is regarded as purely resistive.

Chapter 4 adopts a self-sensing system recognised for IPMCs and successfully implements this concept on a CPC actuator. In this system, voltage drops on electrode layers of a working actuator are registered to determine the position of the actuator. The experimental results yield that such a concept works best as a self-sensing collision detector able to sense objects in its path. However, acquiring precise data on position is challenging due to concurrent processes of input signal propagation along the material as well as mechanically induced change in electrochemical impedance.

Chapters 5 and 6 discuss the similarities and differences of identical self-sensing devices based on different IEAP materials – IPMC and CPC correspondingly.

Uncoupling the sensory information and actuation signal is achieved by patterning of electrode layers of an IEAP. In chapter 5 a special pattern separating each electrode layer of a single IPMC sample into coincident actuator, shielding, and sensor segments is introduced. A sensing signal is obtained by measuring change in electrode resistance, while the shielding section suppresses noise propagating from actuator to sensor. An actuator segment is responsible for bending the whole IEAP device. A mathematical model, taking into account the geometry of patterning, was derived to describe the relation between sensing output and material deflection.

Three different techniques for patterning the platinum electrodes of an IPMC are compared: manual scraping, machining, and laser ablation. While all these methods were sufficient to produce the required patterning, laser ablation proved to be most practical as it allowed removal of platinum simultaneously from both electrodes.

The detailed analysis demonstrates that despite the patterning method, the material remains chemically and physically intact. The choice of method should be argued solely on the precision and cost of the patterning.

The concept of patterning electrodes was utilised on CPC, however an alternate technique for creating different segments for sensing and actuation

was developed. The polymer membrane of CPC was masked prior to spray painting electrodes on it. The segmented CPC actuator was obtained after removing the mask. In spite of the shielding electrode the cross-talk from actuator to sensor remained as a drawback for such a system.

In general, following conclusions can be made in regards of patterning IEAP actuators:

- The IEAP device must be optimised for actuation, *i.e.* the shielding and sensing sections should be as small as possible to have minimal impeding effect on actuation.
- The shielding electrode must provide good conductivity to fully suppress any cross-talk from actuator to sensor.
- Inherently IPMCs can be considered better suited for creating self-sensing IEAP actuators with patterned electrodes as they possess some of the essential qualities by default. A majority of IPMCs have electrodes with very good conductivity, thus, resolving the issue of the shielding electrode. Additionally, a highly convenient method of simultaneous patterning by laser ablation is currently a possibility for only IPMCs. Furthermore, most IPMCs can be easily regenerated if the process of pattern creation should cause the performance of the actuator to decrease.
- When acquiring the sensing signal from the electrode, a balanced bridge circuit of coincident sensing electrodes proved to be irreplaceable in two different situations: for subtracting common mode noise (*i.e.* removing cross-talk between different segments of electrode) and for determining the direction of bending in cases where change of resistance is unidirectional despite the direction of bending.

8. SUMMARY IN ESTONIAN

Ioonsete elektromehaaniliselt aktiivsete polümeeride deformatsioonist sõltuv elektroodi impedants

Elektromehaaniliselt aktiivsed polümeerid (EAP) muudavad oma välist kuju, kui neid elektriliselt stimuleerida; tihti nimetatakse neid ka tehislihasteks. Taolistest materjalidest valmistatud täiturid pakuvad huvi nii mikrolaborseadmetes kui ka loodust matkivas robootikas, sest võimaldavad luua keerukaid ülipisikesi ajameid. Võrreldes tavapäraste elektrimootoritega võimaldavad EAP-d helitut liigutust ning neid saab lõigata konkreetse rakenduse jaoks sobivasse suurusesse. Mitmed elektromehaanilised omadused (avaldatav jõud, liigutuse ulatus jms) on eelseadistatavad juba tehislihaste valmistamise protsessis. Lisaks täituromadustele on enamikul EAP-dest kirjeldatud ka anduromadused, nt materjali väline mehaaniline manipulatsioon on elektrilise signaali kujul tuvastatav. Käesolevas doktoritöös käsitletakse ühte tehislihaste alamklassi – IEAP (ioon-EAP) –, kus mehaaniline koste on tingitud ioonide ümberpaigutumisest mitmekihilises komposiitmaterjalis. Tüüpiliselt on IEAP täitur sümmeetrilise struktuuriga, kus ioonidele läbitav polümeerleht on mõlemalt pinnalt kaetud juhtivast materjalist elektroodidega. Elektroodide vahele rakendatud võrdlemisi madal pinge (kuni 3–4 V) paneb materjali painduma.

IEAP-de rakendamist takistab aga nende materjalide elektromehaaniliste näitajate tugev sõltuvus ümbritseva keskkonna parameetritest (temperatuur, niiskus jne). Seetõttu on EAP-täiturite täppisjuhtimiseks tarvis rakendada tagasidega süsteemi, mis omakorda pärsib EAP-materjalide kasutuselevõttu just miniatuursetes seadmetes, kus tihtipeale pole enam ruumi täiendavale tagasiside andurile. Lahendusena on mitmete EAP-materjalide puhul kirjeldatud n-ö isetundlik täitur. Isetundliku süsteemi korral kasutatakse täiturmaterjali enda anduromadusi tagasiside allikana, kõrvaldades vajaduse täiendava anduri järele.

Käesolevas doktoritöös uuritakse kahte tüüpi painduvate IEAP-materjalide – ioonpolümeer-metallkomposiit (IPMC) ning süsinik-polümeerkomposiit (CPC) – kasutamist eespool kirjeldatud isetundlike täituritena. Kuigi mõlemat tüüpi täiturid on väliselt võrdlemisi sarnased, võib nende tööpõhimõtetes tuvastada mitmeid erinevusi. Doktoritöö seab endale eesmärgiks isetundliku IEAP realiseerimise mõlema materjali baasilt ning lisaks tuua süstemaatilise võrdluse vormis välja peamised erinevused ja sarnasused IPMC ja CPC vahel. Kuna IPMC on pikema ajalooga kui CPC, siis on ka üheks eesmärgiks uurida, kuidas on varasemad IPMC-d käsitlevad tulemused rakendatavad CPC-dele.

Töö sissejuhatavas peatükis kirjeldatakse IEAP-de klassifikatsiooni ning tuuakse näited erinevatest elektroodimaterjalidest, mida on viimase kahekümne aasta jooksul nende loomiseks kasutatud. Muuhulgas tutvustatakse ka erinevaid teooriad, millega selgitatakse käsitletavate täiturite tööpõhimõtet.

Doktoritöö ülejäänud osa võib jagada kolmeks.

a) IPMC- ja CPC-materjalide sensoromaduste analüüs elektrokeemilise impedantsspektroskoopia (EIS) meetodil. Selle eesmärgiks on määratleda

elektriline ekvivalentskeem, mis võimaldab süsinik-polümeerkomposiiti kirjeldada takistitest ja kondensaatoritest koosneva viiteliinina ning määrata nende komponentide sõltuvus materjali deformatsioonist.

b) Isetundliku IPMC kontseptsiooni rakendamine CPC-täiturile, mõõtes elektroodide pingelangusid töötsükli vältel tuvastamaks signaali liigutuse kohta.
c) IPMC- ja CPC-täiturite elektroodide segmenteerimine selliselt, et ühe materjaliriba peal oleksid eraldi täitur- ja andurkomponent.

EIS näitab, et nii IPMC kui ka CPC elektroodi impedants muutub sõltuvalt materjali kõverusraadiusest ehk täituri painutuse ulatusest. Muutuvad nii takistuslik kui ka mahtuvuslik komponent, ent uurides CPC-materjali koostisosasid eraldi, saab järeldada, et CPC elektroodikihti võib vastavas ekvivalentskeemis vaadelda siiski kui puhast takistit.

Nii eksperimendid kui ka arvutisimulatsioonid demonstreerivad, et mõõtes CPC-täituri elektroodide pingelangu, on võimalik tuvastada täituri teele jäävaid takistusi. Kuna aga nimetatud pingelang kirjeldab ka täitursignaali levikut materjalis, mis käitub kui viiteliin, siis on täpne positsioonituvastus raskendatud.

Ühe võimalusena nimetatud probleemi lahendamiseks pakutakse doktoritöös välja elektroodikihi piires täituri ja anduri elektriline eraldamine. Loobudes ainult elektroodimaterjalist säilitab polümeerkarkass täituri ja anduri mehaanilise ühendatuse – seega järgib sensor taolises süsteemis täituri kuju, kuigi need on elektriliselt lahti sidestatud. Kuna sedasi loodud elektroodi osade vahel on siiski täheldatav ka mittesoovitud signaalide ülekandumine, mis on ennekõike tingitud mahtuvuslikust sidestamisest, pakub käesolev töö välja maandatud varjestuselektroodi loomise täituri ja sensori vahele.

Kokkuvõttes saavutatakse süsteem, mille kumbki elektroodikiht koosneb kolmest erinevast alast: täiturist, varjestusest ja sensorist. Andursignaalina kasutatakse varasemalt kirjeldatud nähtust, et elektroodi impedants (mh takistus) muutub sõltuvalt materjali painutusest. Takistuse muutuse mõõtmiseks kasutatakse Wheatstone'i silda, et võimendada erinevate elektroodide takistuse diferentsiaali ning suruda maha võimalikku täiturisignaali ülekostust. Doktoritöös kirjeldatakse ka matemaatiline mudel, mis seob andurelektroodi takistuse materjali geomeetriliste parameetrite kaudu täituri painutusega.

Kirjeldatud isetundliku süsteemi elektroodide eraldamiseks saab valida mitmeid meetodeid. Üldiselt võib meetodid jaotada kaheks: 1) elektroodimaterjali eemaldamine erinevate funktsioonidega osade vahelt või 2) elektroodi valikuline loomine ainult eelnevalt määratud kohtadesse. Doktoritöös käsitletud IPMC-materjali puhul kasutati elektroodi valikulise eemaldamise meetodit, kuna uuritava materjali näol on tegu kommertstootega, mistõttu ei ole tarbijal kontrolli tootmisprotsessi üle. Ent kuna CPC-materjale valmistatakse Tartu Ülikoolis kohapeal, rakendati nende puhul elektroodide valikulise katmise meetodit.

Elektroodimaterjali eemaldamiseks uuriti lisaks mehaanilisele lõikamisele (kraapimine ja freesimine) ka laserablatsiooni (KrF eksimeerlaser). Kõigi nimetatud meetoditega õnnestus luua süsteem, kus täituri liigutus oli tuvastatav andurelektroodidelt mõõdetud signaali abil. Küll aga osutus valmistamisprot-

sessi seisukohalt kõige mugavamaks just laserablatsiooni meetod, mis võimaldas eemaldada elektroodimaterjali samaaegselt mõlemalt pinnalt (kasutatud polümeerkile on nii nähtava valguse kui ka ultraviolettkiirguse spektriosas praktiliselt läbipaistev).

Valminud prototüüpide mehaanilisi ja keemilisi omadusi uuriti nii EIS kui ka FTIR meetodil ning jõuti järeldusele, et valmistamisprotsess ei kahjusta ega muuda polümeeri. Seetõttu saab väita, et elektroodide eraldamiseks sobivaima meetodi valik sõltub peaasjalikult protsessi hinnast ja keerukusest.

CPC korral kaeti polümeerikiht enne elektroodide pealekandmist šablooniga, mis võimaldas jätta osa aladest elektroodilahusega katmata.

Valminud isetundliku IEAP-täituri prototüüpide põhjal saab öelda, et kuna passiivsed osad (nagu andurelement ja varjestus) pärsivad täituri liigutust, tuleb minimeerida nende osakaalu kogu seadmes. Lisaks on seadme edukaks toimimiseks vajalik hea juhtivusega varjestus, nt IPMC puhul on elektroodi enda juhtivus piisav, samas kui CPC puhul on vajalik oluliselt vähenda varjestuselektroodi takistust.

Kuigi antud uurimuses kasutatud materjalidest andis isetundlikus konfiguratsioonis paremaid tulemusi (suurem liigutusulatus, väiksem müra) just IPMC, siis CPC valmistamiseks kasutatud metoodika on ülekantav mikrotäiturite tootmisse tindiprits-trükkimise meetodil.

ACKNOWLEDGEMENTS

First of all I would like to thank my supervisors Dr Andres Punning and Prof Alvo Aabloo for their support and guidance during my studies. In this unique collaboration Andres was always there to help me out with the necessary engineering know-how while Alvo taught me how some of the things in this world actually work.

I value the productive environment of IMS Lab at the University of Tartu – thank you everybody for endless discussions both on- and off-topic.

I would also like to acknowledge my dear Italian colleagues – Prof Salvatore Graziani and Dr Paola Brunetto – for kick-starting my PhD research in Catania during my first year as a doctoral student.

Last but not least, I express gratitude to my family and friends for their continuous support throughout my studies at the university. My special thanks go to Helena for being there for me!

Aitäh kõigile, kes on mind toetanud!

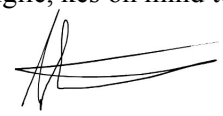

REFERENCES

[1] Bar-Cohen, Y., Electroactive Polymer (EAP) Actuators as Artificial Muscles – Reality, Potential, and Challenges (2nd Edition), SPIE Press (2004).

[2] Carpi, F., De Rossi, D., Kornbluh, R., Pelrine, R., Sommer-Larsen, P., Dielectric Elastomers as Electromechanical Transducers: Fundamentals, Materials, Devices, Models and Applications of an Emerging Electroactive Polymer Technology, Elsevier (2008).

[3] Pugal, D., Jung, K., Aabloo, A., Kim, K. J., "Ionic polymer-metal composite mechanoelectrical transduction: review and perspectives," Polym.Int. 59(3), 279–89 (2010).

[4] Akbari, S., Shea, H., "An array of 100 μm x 100 μm dielectric elastomer actuators with 80% strain for tissue engineering applications," Sensor.Actuat.A-Phys. 186, 236–41 (2012).

[5] Khaldi, A., Plesse, C., Soyer, C., Troadec, D., Vidal, F., Cattan, E., et al., "Micro-beam actuator based on conducting interpenetrating polymer networks: From patterning process to actuation in open air," 16th International Solid-State Sensors, Actuators and Microsystems Conference (TRANSDUCERS) 462–5 (2011).

[6] Dosch, J. J., Inman, D. J., Garcia, E., "A Self-Sensing Piezoelectric Actuator for Collocated Control," J.Intel.Mat.Syst.Str. 3(1), 166–85 (1992).

[7] Jung, K., Kim, K. J., Choi, H. R., "A self-sensing dielectric elastomer actuator," Sensor.Actuat.A-Phys. 143(2), 343–51 (2008).

[8] Tiwari, R., Garcia, E., "The state of understanding of ionic polymer metal composite architecture: a review," Smart Mater.Struct. 20(8), 083001 (2011).

[9] Hao, L., Li, Z., "Modeling and adaptive inverse control of hysteresis and creep in ionic polymer–metal composite actuators," Smart Mater.Struct. 19(2), 025014 (2010).

[10] Hao, L., Sun, Z., Li, Z., Su, Y., Gao, J., "A novel adaptive force control method for IPMC manipulation," Smart Mater.Struct. 21(7), 075016 (2012).

[11] Baughman, R. H., Cui, C., Zakhidov, A. A., Iqbal, Z., Barisci, J. N., Spinks, G. M., et al., "Carbon nanotube actuators," Science 284(5418), 1340–4 (1999).

[12] Bennett, M. D., Leo, D. J., "Ionic liquids as stable solvents for ionic polymer transducers," Sensor.Actuat.A-Phys. 115(1), 79–90 (2004).

[13] Fukushima, T., Asaka, K., Kosaka, A., Aida, T., "Fully Plastic Actuator through Layer-by-Layer Casting with Ionic-Liquid-Based Bucky Gel," Angew.Chem.Int. Edit. 117(16), 2462–5 (2005).

[14] Akle, B. J., Bennett, M. D., Leo, D. J., "High-strain ionomeric–ionic liquid electroactive actuators," Sensor.Actuat.A-Phys. 126(1), 173–81 (2006).

[15] Akle, B. J., Leo, D. J., Hickner, M. A., McGrath, J. E., "Correlation of capacitance and actuation in ionomeric polymer transducers," J.Mater.Sci. 40(14), 3715–24 (2005).

[16] Beguin, F., Frackowiak, E., Carbons for Electrochemical Energy Storage and Conversion Systems, CRC Press (2009).

[17] Nemat-Nasser, S., "Micromechanics of actuation of ionic polymer-metal composites," J.Appl.Phys. 92(5), 2899–915 (2002).

[18] Zheng, J., Moganty, S. S., Goonetilleke, P. C., Baltus, R. E., Roy, D., "A Comparative Study of the Electrochemical Characteristics of [Emim+][BF4−] and

[Bmim+][BF4−] Ionic Liquids at the Surfaces of Carbon Nanotube and Glassy Carbon Electrodes," J.Phys.Chem.C 115(15), 7527–37 (2011).
[19] Takeuchi, I., Asaka, K., Kiyohara, K., Sugino, T., Terasawa, N., Mukai, K., et al., "Electromechanical behavior of fully plastic actuators based on bucky gel containing various internal ionic liquids," Electrochim. Acta 54(6), 1762–8 (2009).
[20] Shahinpoor, M., Kim, K. J., "Ionic polymer-metal composites. I. Fundamentals," Smart Mater. Struct. 10(4), 819–33 (2001).
[21] Shahinpoor, M., Bar-Cohen, Y., Simpson, J. O., Smith, J., "Ionic polymer-metal composites (IPMCs) as biomimetic sensors, actuators and artificial muscles-a review," Smart Mater.Struct. 7(6), 15–30 (1998).
[22] Palmre, V., Brandell, D., Mäeorg, U., Torop, J., Volobujeva, O., Punning, A., et al., "Nanoporous carbon-based electrodes for high strain ionomeric bending actuators," Smart Mater.Struct. 18(9), 095028 (2009).
[23] Shahinpoor, M., Kim, K. J., "The effect of surface-electrode resistance on the performance of ionic polymer-metal composite (IPMC) artificial muscles," Smart Mater.Struct. 9(4), 543–51 (2000).
[24] Stoimenov, B. L., Rossiter, J., Mukai, T., Asaka, K., "Frequency response of anisotropic ionic polymer metal composites (IPMC) transducers," Proc.SPIE 6927, 69270K (2008).
[25] Kim, K. J., Shahinpoor, M., "Ionic polymer–metal composites: II. Manufacturing techniques," Smart Mater.Struct. 12(1), 65–79 (2003).
[26] Oguro, K., Fujiwara, N., Asaka, K., Onishi, K., Sewa, S., "Polymer electrolyte actuator with gold electrodes," Proc.SPIE 3669, 64–71 (1999).
[27] Bennett, M. D., Leo, D. J., "Manufacture and characterization of ionic polymer transducers employing non-precious metal electrodes," Smart Mater.Struct. 12(3), 424–36 (2003).
[28] Johanson, U., Mäeorg, U., Sammelselg, V., Brandell, D., Punning, A., Kruusmaa, M., et al., "Electrode reactions in Cu–Pt coated ionic polymer actuators," Sensor. Actuat.B-Chem. 131(1), 340–6 (2008).
[29] Uchida, M., Taya, M., "Solid polymer electrolyte actuator using electrode reaction," Polymer 42(22), 9281–5 (2001).
[30] Kim, S., Kim, K. J., "Palladium buffer-layered high performance ionic polymer–metal composites," Smart Mater.Struct. 17(3), 035011 (2008).
[31] Shahinpoor, M., Kim, K. J., "Novel ionic polymer–metal composites equipped with physically loaded particulate electrodes as biomimetic sensors, actuators and artificial muscles," Sensor.Actuat.A-Phys. 96(2–3), 125–32 (2002).
[32] Tamagawa, H., Nogata, F., Watanabe, T., Abe, A., Yagasaki, K., Jin, J.-Y., "Influence of metal plating treatment on the electric response of Nafion," J.Mater. Sci. 38(5), 1039–44 (2003).
[33] Kim, S., Tiwari, R., Kim, K. J., "A Novel Ionic Polymer Metal ZnO Composite (IPMZC)," Sensors 11(5), 4674–87 (2011).
[34] Akle, B. J., "Characterization and Modeling of the Ionomer-Conductor Interface in Ionic Polymer Transducers," PhD dissertation, Virginia Polytechnic Institute and State University (2005).
[35] Akle, B., Bennett, M., Leo, D., Wiles, K., McGrath, J., "Direct assembly process: a novel fabrication technique for large strain ionic polymer transducers," J.Mater.Sci. 42(16), 7031–41 (2007).

[36] Palmre, V., Lust, E., Jänes, A., Koel, M., Peikolainen, A.-L., Torop, J., et al., "Electroactive polymer actuators with carbon aerogel electrodes," J.Mater.Chem. 21(8), 2577–83 (2011).
[37] Landi, B. J., Raffaelle, R. P., Heben, M. J., Alleman, J. L., VanDerveer, W., Gennett, T., "Single Wall Carbon Nanotube−Nafion Composite Actuators," Nano Lett. 2(11), 1329–32 (2002).
[38] Lian, H., Qian, W., Estevez, L., Liu, H., Liu, Y., Jiang, T., et al., "Enhanced actuation in functionalized carbon nanotube–Nafion composites," Sensor.Actuat. B-Chem. 156(1), 187–93 (2011).
[39] Lee, D. Y., Lee, M., Kim, K. J., Heo, S., Kim, B., Lee, S., "Effect of multiwalled carbon nanotube (M-CNT) loading on M-CNT distribution behavior and the related electromechanical properties of the M-CNT dispersed ionomeric nanocomposites," Surf.Coat.Tech. 200(5–6), 1920–5 (2005).
[40] Oh, I., Jung, J., Jeon, J., Vadahanambi, S., "Electro-chemo-mechanical characteristics of fullerene-reinforced ionic polymer–metal composite transducers," Smart Mater.Struct. 19(7), 075009 (2010).
[41] Jung, J., Jeon, J., Sridhar, V., Oh, I., "Electro-active graphene–Nafion actuators," Carbon 49(4), 1279–89 (2011).
[42] Lian, Y., Liu, Y., Jiang, T., Shu, J., Lian, H., Cao, M., "Enhanced Electromechanical Performance of Graphite Oxide-Nafion Nanocomposite Actuator," J.Phys.Chem.C 114(21), 9659–63 (2010).
[43] Mukai, K., Asaka, K., Sugino, T., Kiyohara, K., Takeuchi, I., Terasawa, N., et al., "Highly Conductive Sheets from Millimeter-Long Single-Walled Carbon Nanotubes and Ionic Liquids: Application to Fast-Moving, Low-Voltage Electromechanical Actuators Operable in Air," Adv.Mater. 21(16), 1582–5 (2009).
[44] Torop, J., Arulepp, M., Leis, J., Punning, A., Johanson, U., Palmre, V., et al., "Nanoporous Carbide-Derived Carbon Material-Based Linear Actuators," Materials 3(1), 9–25 (2009).
[45] Torop, J., Palmre, V., Arulepp, M., Sugino, T., Asaka, K., Aabloo, A., "Flexible supercapacitor-like actuator with carbide-derived carbon electrodes," Carbon 49(9), 3113–9 (2011).
[46] Kaasik, F., Torop, J., Peikolainen, A.-L., Koel, M., Aabloo, A., "Carbon aerogel based electrode material for EAP actuators," Proc.SPIE 7976, 79760O (2011).
[47] Sadeghipour, K., Salomon, R., Neogi, S., "Development of a novel electrochemically active membrane and 'smart' material based vibration sensor/damper," Smart Mater.Struct. 1(2), 172–9 (1992).
[48] Kamamichi, N., Yamakita, M., Asaka, K., Zhi-Wei Luo, Mukai, T., "Sensor Property of a Novel EAP Device with Ionic-liquid-based Bucky Gel," Proc.IEEE Sensors, 221–4 (2007).
[49] Must, I., Kaasik, F., Põldsalu, I., Johanson, U., Punning, A., Aabloo, A., "A carbide-derived carbon laminate used as a mechanoelectrical sensor," Carbon 50(2), 535–41 (2012).
[50] Bonomo, C., Fortuna, L., Giannone, P., Graziani, S., "A method to characterize the deformation of an IPMC sensing membrane," Sensor.Actuat.A-Phys. 123–124, 146–54 (2005).
[51] Punning, A., Kruusmaa, M., Aabloo, A., "Surface resistance experiments with IPMC sensors and actuators," Sensor.Actuat.A-Phys. 133(1), 200–9 (2007).
[52] Bar-Cohen, Y., Biomimetics: Nature-Based Innovation, CRC Press (2011).
[53] Carpi, F., Smela, E., Biomedical Applications of Electroactive Polymer Actuators, John Wiley & Sons Ltd (2009).

[54] Shahinpoor, M., Kim, K. J., “Ionic polymer-metal composites: IV. Industrial and medical applications,” Smart Mater.Struct. 14(1), 197–214 (2005).
[55] Tsiakmakis, K., Brufau-Penella, J., Puig-Vidal, M., Laopoulos, T., “A Camera Based Method for the Measurement of Motion Parameters of IPMC Actuators,” IEEE T.Instrum.Meas. 58(8), 2626–33 (2009).
[56] Anton, M., Aabloo, A., Punning, A., Kruusmaa, M., “A mechanical model of a non-uniform ionomeric polymer metal composite actuator,” Smart Mater.Struct. 17(2), 025004 (2008).
[57] Chen, Z., Ki-Yong Kwon, Tan, X., “Integrated IPMC/PVDF sensory actuator and its validation in feedback control,” Sensor.Actuat.A-Phys. 144(2), 231–41 (2008).
[58] Leang, K. K., Shan, Y., Song, S., Kim, K. J., “Integrated Sensing for IPMC Actuators Using Strain Gages for Underwater Applications,” IEEE-ASME T.Mech. 17(2), 345–55 (2012).
[59] Chen, Z., Shen, Y., Xi, N., Tan, X., “Integrated sensing for ionic polymer–metal composite actuators using PVDF thin films,” Smart Mater.Struct. 16(2), S262–71 (2007).
[60] Hunt, A., Chen, Z., Tan, X., Kruusmaa, M., “Feedback Control of a Coupled IPMC (Ionic Polymer-Metal Composite) Sensor-Actuator,” ASME 2009 Dynamic Systems and Control Conference 1, 485–91 (2009).
[61] Bonomo, C., Fortuna, L., Giannone, P., Graziani, S., “A sensor-actuator integrated system based on IPMCs,” Proc.IEEE Sensors 1, 489–92 (2004).
[62] Nakadoi, H., Sera, A., Yamakita, M., Asaka, K., Zhi-Wei, L., Ito, K., “Integrated actuator-sensor system on patterned IPMC film: consideration of electoric interference,” 4th IEEE International Conference on Mechatronics (ICM2007), 1–6 (2007).
[63] Anderson, E. H., Hagood, N. W., “Simultaneous Piezoelectric Sensing/ Actuation: Analysis And Application To Controlled Structures,” J.Sound Vib. 174(5), 617–39 (1994).
[64] Lan, C.-C., Lin, C.-M., Fan, C.-H., “A Self-Sensing Microgripper Module With Wide Handling Ranges,” IEEE-ASME T.Mech. 16(1), 141–50 (2011).
[65] Punning, A., Kruusmaa, M., Aabloo, A., “A self-sensing ion conducting polymer metal composite (IPMC) actuator,” Sensor. Actuat.A-Phys. 136(2), 656–64 (2007).
[66] Otero, T. F., “Soft, wet, and reactive polymers. Sensing artificial muscles and conformational energy,” J.Mater.Chem. 19(6), 681–9 (2009).
[67] Bao, X., Bar-Cohen, Y., Lih, S., “Measurements and macro models of ionomeric polymer-metal composites (IPMC),” Proc.SPIE 4695, 220–7 (2002).
[68] Bonomo, C., Fortuna, L., Giannone, P., Graziani, S., Strazzeri, S., “A nonlinear model for ionic polymer metal composites as actuators,” Smart Mater.Struct. 16(1), 1–12 (2007).
[69] Jung, K., Nam, J., Choi, H., “Investigations on actuation characteristics of IPMC artificial muscle actuator,” Sensor.Actuat.A-Phys 107(2), 183–92 (2003).
[70] Paquette, J. W., Kim, K. J., Nam, J., Tak, Y. S., “An Equivalent Circuit Model for Ionic Polymer-Metal Composites and their Performance Improvement by a Clay-Based Polymer Nano-Composite Technique,” J.Intel.Mat.Syst.Str. 14(10), 633–42 (2003).
[71] Kanno, R., Tadokoro, S., Takamori, T., Hattori, M., Oguro, K., “Linear approximate dynamic model of ICPF (ionic conducting polymer gel film) actuator,” IEEE Int.Conf.Robot. 1, 219–25 (1996).

[72] Chen, Z., Tan, X., “A Control-Oriented and Physics-Based Model for Ionic Polymer – Metal Composite Actuators,” IEEE-ASME T.Mech. 13(5), 519–29 (2008).
[73] Takagi, K., Nakabo, Y., Luo, Z., Asaka, K., “On a distributed parameter model for electrical impedance of ionic polymer,” Proc.SPIE 6524, 652416 (2007).
[74] Punning, A., Johanson, U., Anton, M., Aabloo, A., Kruusmaa, M., “A distributed model of ionomeric polymer metal composite,” J.Intel.Mat.Syst.Str. 20(14), 1711–24 (2009).
[75] Must, I., Kruusamäe, K., Johanson, U., Tamm, T., Punning, A., Aabloo, A., “Characterisation of electromechanically active polymers using electrochemical impedance spectroscopy,” Lecture Notes on Impedance Spectroscopy: Measurement, Modeling and Applications 2, 113–21 (2012).
[76] Takeuchi, I., Asaka, K., Kiyohara, K., Sugino, T., Mukai, K., Randriamahazaka, H., “Electrochemical Impedance Spectroscopy and Electromechanical Behavior of Bucky-Gel Actuators Containing Ionic Liquids,” J.Phys.Chem.C 114(34), 14627–34 (2010).
[77] Randriamahazaka, H., Asaka, K., “Electromechanical Analysis by Means of Complex Capacitance of Bucky-Gel Actuators Based on Single-Walled Carbon Nanotubes and an Ionic Liquid,” J.Phys.Chem.C 114(41), 17982–8 (2010).
[78] Torop, J., Kaasik, F., Sugino, T., Aabloo, A., Asaka, K., “Electromechanical characteristics of actuators based on carbide-derived carbon,” Proc.SPIE 7642, 76422A (2010).
[79] Nakabo, Y., Mukai, T., Asaka, K., “Biomimetic soft robots with artificial muscles,” Proc.SPIE 5648, 132–44 (2004).
[80] Nakabo, Y., Mukai, T., Asaka, K., “Kinematic Modeling and Visual Sensing of Multi-DOF Robot Manipulator with Patterned Artificial Muscle,” IEEE Int. Conf. Robot 4315–20 (2005).
[81] Rossiter, J. M., Stoimenov, B. L., Mukai, T., “A linear actuator from a single ionic polymer-metal composite (IPMC) strip,” Proc.SPIE 6524, 65241B (2007).
[82] Stoimenov, B. L., Rossiter, J. M., Mukai, T., “Manufacturing of ionic polymer-metal composites (IPMCs) that can actuate into complex curves,” Proc.SPIE 6524, 65240T (2007).
[83] Jeon, J., Yeom, S., Oh, I., “Fabrication and actuation of ionic polymer metal composites patterned by combining electroplating with electroless plating,” Compos-Part A-Appl.S 39(4), 588–96 (2008).
[84] Riddle, R. O., Jung, Y., Kim, S., Song, S., Stolpman, B., Kim, K. J., et al., “Sectored-electrode IPMC actuator for bending and twisting motion,” Proc.SPIE 7642, 764221 (2010).
[85] Sareh, S., Conn, A. T., Rossiter, J. M., Ieropoulos, I., Walters, P., “Optimization of bio-inspired multi-segment IPMC cilia,” Proc.SPIE 7642, 76421S (2010).
[86] Rossiter, J., Mukai, T., “Electrostatic and thermal segmentation of multi-segment IPMC sensor-actuators,” Proc.SPIE 7976, 79761C (2011).
[87] Kim, K. J., Pugal, D., Leang, K. K., “A Twistable Ionic Polymer-Metal Composite Artificial Muscle for Marine Applications,” Mar.Technol.Soc.J. 45(4), 83–98 (2011).
[88] Konyo, M., Konishi, Y., Tadokoro, S., Kishima, T., “Development of velocity sensor using ionic polymer-metal composites,” Proc.SPIE 5385, 307–18 (2004).
[89] Kamamichi, N., Stoimenov, B., Mukai, T., Asaka, K., “A Sensor-Actuator Integrated System with a Patterned IPMC – the interference of actuation to the

sensing signal –," SI2006: SICE System Integration Division Annual Conference, 175–6 (2006).
[90] De Almeida, S. H., Kawano, Y., "Ultraviolet-visible spectra of Nafion membrane," Eur. Polym. J. 33(8), 1307–11 (1997).
[91] Chae, J., Jin, H., Jain, K., "Large-area, high-speed patterning of carbon nanotubes using material-assisted excimer laser photoablation," Mater Lett 63(21), 1823–5 (2009).
[92] Liang, Z., Chen, W., Liu, J., Wang, S., Zhou, Z., Li, W., et al., "FT-IR study of the microstructure of Nafion® membrane," J.Membrane Sci. 233(1–2), 39–44 (2004).
[93] Ludvigsson, M., Lindgren, J., Tegenfeldt, J., "FTIR study of water in cast Nafion films," Electrochim.Acta 45(14), 2267–71 (2000).
[94] Lin, H. K., Lin, R. C., Li, C. H., "Etching processes of transparent carbon nanotube thin films using laser technologies," Thin Solid Films 518(24), 7253–7 (2010).
[95] Walton, M. D., Kim, Y. S., Jan, C. J., McConnel, E. P., Everett, W. N., Grunlan, J. C., "Deposition and patterning of conductive carbon black thin films," Synthetic Met. 157(16–17), 632–9 (2007).
[96] Sangwan, V. K., Ballarotto, V. W., Hines, D. R., Fuhrer, M. S., Williams, E. D., "Controlled growth, patterning and placement of carbon nanotube thin films," Solid State Electron. 54(10), 1204–10 (2010).
[97] Roch, T., Beyer, E., Lasagni, A., "Surface modification of thin tetrahedral amorphous carbon films by means of UV direct laser interference patterning," Diam.Relat.Mater. 19(12), 1472–7 (2010).
[98] Mionic, M., Pataky, K., Gaal, R., Magrez, A., Brugger, J., Forro, L., "Carbon nanotubes-SU8 composite for flexible conductive inkjet printable applications," J.Mater.Chem. 22(28), 14030–4 (2012).
[99] Palmre, V., Torop, J., Arulepp, M., Sugino, T., Asaka, K., Jänes, A., et al., "Impact of carbon nanotube additives on carbide-derived carbon-based electroactive polymer actuators," Carbon 50(12), 4351–8 (2012).
[100] Kruusamäe, K., Punning, A., Aabloo, A., "Self-sensing properties of carbon-polymer composite (CPC) actuators," Proc.SPIE 7976, 79760Q (2011).

PUBLICATIONS

CURRICULUM VITAE

Name: Karl Kruusamäe
Date of birth: 11.10.1984
Citizenship: Estonian
E-mail: karl.kruusamae@ut.ee

Education:

2008 onwards	University of Tartu, Faculty of Science and Technology, doctoral studies in Physics
2009–2009	University of Catania, Faculty of Engineering, exchange doctoral student
2006–2008	University of Tartu, Faculty of Science and Technology, MSc in Engineering (Information Technology)
2003–2006	University of Tartu, Faculty of Physics and Chemistry, BSc in Engineering (Information Technology)

Employment:

2009 onwards	University of Tartu, Faculty of Science and Technology, Programme Manager for Computer Engineering

Publications:

– Journal articles

Kruusamäe, K.; Punning, A.; Aabloo, A. (2012) *Electrical Model of a Carbon-Polymer Composite (CPC) Collision Detector*, Sensors 12(2), 1950–1966.

Kruusamäe, K.; Brunetto, P.; Graziani, S.; Fortuna, L.; Kodu, M.; Jaaniso, R.; Punning, A.; Aabloo, A. (2011) *Electromechanical model for a self-sensing ionic polymer-metal composite actuating device with patterned surface electrodes*, Smart Materials and Structures 20(12), 124001.

Kruusamäe, K.; Brunetto, P.; Graziani S.; Punning, A.; Di Pasquale, G.; Aabloo, A. (2010) *Self-sensing IPMC actuating device with patterned surface electrodes*, Polymer International 59(3), 300–304.

– Conference proceedings

Kontio, J.; Granholm, P.; Valmu, H.; Mäntykoski, J.; **Kruusamäe, K.**; Aukstuoliene, M.; Savulioniene, L.; Hussmann, P.M.; Edström, K. (2012) *Supporting programme development with self- and cross evaluations – results from an international quality assurance project*, Proceedings of International Conference on Engineering Education 2012 (ICEE 2012), 816 - 823.

Kruusamäe, K. (2012) *Artificial muscles: more than just actuators for micro-robots*, Annual of Estonian Physical Society 22, 60–72 (in Estonian).

Must, I.; **Kruusamäe, K.**; Johanson, U.; Tamm, T.; Punning, A.; Aabloo, A. (2012) *Characterisation of electromechanically active polymers using*

electrochemical impedance spectroscopy, Lecture Notes on Impedance Spectroscopy: Measurement, Modeling and Applications 2, Olfa Kanoun (Ed.), CRC Press, 113–121

Kruusamäe, K.; Punning, A.; Aabloo, A. (2011) *Self-sensing properties of carbon-polymer composite (CPC) actuators*, Proceedings of SPIE 7976, 79760Q.

Kruusamäe, K.; Brunetto, P.; Graziani, S.; Fortuna, L.; Kodu, M.; Jaaniso, R.; Punning, A.; Aabloo, A. (2010) *Experiments with self-sensing IPMC actuating device*, Proceedings of SPIE 7642, 76420V.

Kruusamäe, K.; Punning, A.; Kruusmaa, M.; Aabloo, A. (2009) *Dynamical variation of the impedances of IPMC*, Proceedings of SPIE 7287, 72870V.

ELULOOKIRJELDUS

Nimi: Karl Kruusamäe
Sünniaeg: 11.10.1984
Kodakondsus: Eesti
E-mail: karl.kruusamae@ut.ee

Hariduskäik:

alates 2008	Tartu Ülikool, loodus- ja tehnoloogiateaduskond, füüsika doktorantuur
2009–2009	Catania Ülikool, tehnikateaduskond, stipendiaat
2006–2008	Tartu Ülikool, loodus- ja tehnoloogiateaduskond, tehnikateaduse magister infotehnoloogias
2003–2006	Tartu Ülikool, füüsika-keemiateaduskond, tehnikateaduse bakalaureus infotehnoloogias

Teenistuskäik:

alates 2009	Tartu Ülikool, loodus- ja tehnoloogiateaduskond, arvutitehnika programmijuht

Publikatsioonid:

– Ajakirjaartiklid

Kruusamäe, K.; Punning, A.; Aabloo, A. (2012) *Electrical Model of a Carbon-Polymer Composite (CPC) Collision Detector*, Sensors 12(2), 1950–1966.

Kruusamäe, K.; Brunetto, P.; Graziani, S.; Fortuna, L.; Kodu, M.; Jaaniso, R.; Punning, A.; Aabloo, A. (2011) *Electromechanical model for a self-sensing ionic polymer-metal composite actuating device with patterned surface electrodes*, Smart Materials and Structures 20(12), 124001.

Kruusamäe, K.; Brunetto, P.; Graziani S.; Punning, A.; Di Pasquale, G.; Aabloo, A. (2010) *Self-sensing IPMC actuating device with patterned surface electrodes*, Polymer International 59(3), 300–304.

– Kogumikuartiklid

Kontio, J.; Granholm, P.; Valmu, H.; Mäntykoski, J.; **Kruusamäe, K.**; Aukstuoliene, M.; Savulioniene, L.; Hussmann, P.M.; Edström, K. (2012) *Supporting programme development with self- and cross evaluations – results from an international quality assurance project*, Proceedings of International Conference on Engineering Education 2012 (ICEE 2012), 816–823.

Kruusamäe, K. (2012) *Tehislihased: ajamid mikrorobotitele, kuid mitte ainult*, Eesti Füüsika Seltsi aastaraamat 2011, XXII aastakäik, 60–72.

Must, I.; **Kruusamäe, K.**; Johanson, U.; Tamm, T.; Punning, A.; Aabloo, A. (2012) *Characterisation of electromechanically active polymers using electrochemical impedance spectroscopy*, Lecture Notes on Impedance

Spectroscopy: Measurement, Modeling and Applications 2, Olfa Kanoun (Ed.), CRC Press, 113–121

Kruusamäe, K.; Punning, A.; Aabloo, A. (2011) *Self-sensing properties of carbon-polymer composite (CPC) actuators*, Proceedings of SPIE 7976, 79760Q.

Kruusamäe, K.; Brunetto, P.; Graziani, S.; Fortuna, L.; Kodu, M.; Jaaniso, R.; Punning, A.; Aabloo, A. (2010) *Experiments with self-sensing IPMC actuating device*, Proceedings of SPIE 7642, 76420V.

Kruusamäe, K.; Punning, A.; Kruusmaa, M.; Aabloo, A. (2009) *Dynamical variation of the impedances of IPMC*, Proceedings of SPIE 7287, 72870V.

DISSERTATIONES PHYSICAE UNIVERSITATIS TARTUENSIS

1. **Andrus Ausmees.** XUV-induced electron emission and electron-phonon interaction in alkali halides. Tartu, 1991.
2. **Heiki Sõnajalg.** Shaping and recalling of light pulses by optical elements based on spectral hole burning. Tartu, 1991.
3. **Sergei Savihhin.** Ultrafast dynamics of F-centers and bound excitons from picosecond spectroscopy data. Tartu, 1991.
4. **Ergo Nõmmiste.** Leelishalogeniidide röntgenelektronemissioon kiiritamisel footonitega energiaga 70–140 eV. Tartu, 1991.
5. **Margus Rätsep.** Spectral gratings and their relaxation in some low-temperature impurity-doped glasses and chrystals. Tartu, 1991.
6. **Tõnu Pullerits.** Primary energy transfer in photosynthesis. Model calculations. Tartu, 1991.
7. **Olev Saks.** Attoampri diapasoonis voolude mõõtmise füüsikalised alused. Tartu, 1991.
8. **Andres Virro.** AlGaAsSb/GaSb heterostructure injection lasers. Tartu, 1991.
9. **Hans Korge.** Investigation of negative point discharge in pure nitrogen at atmospheric pressure. Tartu, 1992.
10. **Jüri Maksimov.** Nonlinear generation of laser VUV radiation for high-resolution spectroscopy. Tartu, 1992.
11. **Mark Aizengendler.** Photostimulated transformation of aggregate defects and spectral hole burning in a neutron-irradiated sapphire. Tartu, 1992.
12. **Hele Siimon.** Atomic layer molecular beam epitaxy of A^2B^6 compounds described on the basis of kinetic equations model. Tartu, 1992.
13. **Tõnu Reinot.** The kinetics of polariton luminescence, energy transfer and relaxation in anthracene. Tartu, 1992.
14. **Toomas Rõõm.** Paramagnetic H^{2-} and F^+ centers in CaO crystals: spectra, relaxation and recombination luminescence. Tallinn, 1993.
15. **Erko Jalviste.** Laser spectroscopy of some jet-cooled organic molecules. Tartu, 1993.
16. **Alvo Aabloo.** Studies of crystalline celluloses using potential energy calculations. Tartu, 1994.
17. **Peeter Paris.** Initiation of corona pulses. Tartu, 1994.
18. **Павел Рубин.** Локальные дефектные состояния в CuO_2 плоскостях высокотемпературных сверхпроводников. Тарту, 1994.
19. **Olavi Ollikainen.** Applications of persistent spectral hole burning in ultrafast optical neural networks, time-resolved spectroscopy and holographic interferometry. Tartu, 1996.
20. **Ülo Mets.** Methodological aspects of fluorescence correlation spectroscopy. Tartu, 1996.
21. **Mikhail Danilkin.** Interaction of intrinsic and impurity defects in CaS:Eu luminophors. Tartu, 1997.

22. **Ирина Кудрявцева.** Создание и стабилизация дефектов в кристаллах KBr, KCl, RbCl при облучении ВУФ-радиацией. Тарту, 1997.
23. **Andres Osvet.** Photochromic properties of radiation-induced defects in diamond. Tartu, 1998.
24. **Jüri Örd.** Classical and quantum aspects of geodesic multiplication. Tartu, 1998.
25. **Priit Sarv.** High resolution solid-state NMR studies of zeolites. Tartu, 1998.
26. **Сергей Долгов.** Электронные возбуждения и дефектообразование в некоторых оксидах металлов. Тарту, 1998.
27. **Kaupo Kukli.** Atomic layer deposition of artificially structured dielectric materials. Tartu, 1999.
28. **Ivo Heinmaa.** Nuclear resonance studies of local structure in $RBa_2Cu_3O_{6+x}$ compounds. Tartu, 1999.
29. **Aleksander Shelkan.** Hole states in CuO_2 planes of high temperature superconducting materials. Tartu, 1999.
30. **Dmitri Nevedrov.** Nonlinear effects in quantum lattices. Tartu, 1999.
31. **Rein Ruus.** Collapse of 3d (4f) orbitals in 2p (3d) excited configurations and its effect on the x-ray and electron spectra. Tartu, 1999.
32. **Valter Zazubovich.** Local relaxation in incommensurate and glassy solids studied by Spectral Hole Burning. Tartu, 1999.
33. **Indrek Reimand.** Picosecond dynamics of optical excitations in GaAs and other excitonic systems. Tartu, 2000.
34. **Vladimir Babin.** Spectroscopy of exciton states in some halide macro- and nanocrystals. Tartu, 2001.
35. **Toomas Plank.** Positive corona at combined DC and AC voltage. Tartu, 2001.
36. **Kristjan Leiger.** Pressure-induced effects in inhomogeneous spectra of doped solids. Tartu, 2002.
37. **Helle Kaasik.** Nonperturbative theory of multiphonon vibrational relaxation and nonradiative transitions. Tartu, 2002.
38. **Tõnu Laas.** Propagation of waves in curved spacetimes. Tartu, 2002.
39. **Rünno Lõhmus.** Application of novel hybrid methods in SPM studies of nanostructural materials. Tartu, 2002.
40. **Kaido Reivelt.** Optical implementation of propagation-invariant pulsed free-space wave fields. Tartu, 2003.
41. **Heiki Kasemägi.** The effect of nanoparticle additives on lithium-ion mobility in a polymer electrolyte. Tartu, 2003.
42. **Villu Repän.** Low current mode of negative corona. Tartu, 2004.
43. **Алексей Котлов.** Оксианионные диэлектрические кристаллы: зонная структура и электронные возбуждения. Tartu, 2004.
44. **Jaak Talts.** Continuous non-invasive blood pressure measurement: comparative and methodological studies of the differential servo-oscillometric method. Tartu, 2004.
45. **Margus Saal.** Studies of pre-big bang and braneworld cosmology. Tartu, 2004.

46. **Eduard Gerškevitš.** Dose to bone marrow and leukaemia risk in external beam radiotherapy of prostate cancer. Tartu, 2005.
47. **Sergey Shchemelyov.** Sum-frequency generation and multiphoton ionization in xenon under excitation by conical laser beams. Tartu, 2006.
48. **Valter Kiisk.** Optical investigation of metal-oxide thin films. Tartu, 2006.
49. **Jaan Aarik.** Atomic layer deposition of titanium, zirconium and hafnium dioxides: growth mechanisms and properties of thin films. Tartu, 2007.
50. **Astrid Rekker.** Colored-noise-controlled anomalous transport and phase transitions in complex systems. Tartu, 2007.
51. **Andres Punning.** Electromechanical characterization of ionic polymer-metal composite sensing actuators. Tartu, 2007.
52. **Indrek Jõgi.** Conduction mechanisms in thin atomic layer deposited films containing TiO_2. Tartu, 2007.
53. **Aleksei Krasnikov.** Luminescence and defects creation processes in lead tungstate crystals. Tartu, 2007.
54. **Küllike Rägo.** Superconducting properties of MgB_2 in a scenario with intra- and interband pairing channels. Tartu, 2008.
55. **Els Heinsalu.** Normal and anomalously slow diffusion under external fields. Tartu, 2008.
56. **Kuno Kooser.** Soft x-ray induced radiative and nonradiative core-hole decay processes in thin films and solids. Tartu, 2008.
57. **Vadim Boltrushko.** Theory of vibronic transitions with strong nonlinear vibronic interaction in solids. Tartu, 2008.
58. **Andi Hektor.** Neutrino Physics beyond the Standard Model. Tartu, 2008.
59. **Raavo Josepson.** Photoinduced field-assisted electron emission into gases. Tartu, 2008.
60. **Martti Pärs.** Study of spontaneous and photoinduced processes in molecular solids using high-resolution optical spectroscopy. Tartu, 2008.
61. **Kristjan Kannike.** Implications of neutrino masses. Tartu, 2008.
62. **Vigen Issahhanjan.** Hole and interstitial centres in radiation-resistant MgO single crystals. Tartu, 2008.
63. **Veera Krasnenko.** Computational modeling of fluorescent proteins. Tartu, 2008.
64. **Mait Müntel.** Detection of doubly charged higgs boson in the CMS detector. Tartu, 2008.
65. **Kalle Kepler.** Optimisation of patient doses and image quality in diagnostic radiology. Tartu, 2009.
66. **Jüri Raud.** Study of negative glow and positive column regions of capillary HF discharge. Tartu, 2009.
67. **Sven Lange.** Spectroscopic and phase-stabilisation properties of pure and rare-earth ions activated ZrO_2 and HfO_2. Tartu, 2010.
68. **Aarne Kasikov.** Optical characterization of inhomogeneous thin films. Tartu, 2010.

69. **Heli Valtna-Lukner.** Superluminally propagating localized optical pulses. Tartu, 2010.
70. **Artjom Vargunin.** Stochastic and deterministic features of ordering in the systems with a phase transition. Tartu, 2010.
71. **Hannes Liivat.** Probing new physics in e+e− annihilations into heavy particles via spin orientation effects. Tartu, 2010.
72. **Tanel Mullari.** On the second order relativistic deviation equation and its applications. Tartu, 2010.
73. **Aleksandr Lissovski.** Pulsed high-pressure discharge in argon: spectroscopic diagnostics, modeling and development. Tartu, 2010.
74. **Aile Tamm.** Atomic layer deposition of high-permittivity insulators from cyclopentadienyl-based precursors. Tartu, 2010.
75. **Janek Uin.** Electrical separation for generating standard aerosols in a wide particle size range. Tartu, 2011.
76. **Svetlana Ganina.** Hajusandmetega ülesanded kui üks võimalus füüsikaõppe efektiivsuse tõstmiseks. Tartu, 2011
77. **Joel Kuusk.** Measurement of top-of-canopy spectral reflectance of forests for developing vegetation radiative transfer models. Tartu, 2011.
78. **Raul Rammula**. Atomic layer deposition of HfO_2 – nucleation, growth and structure development of thin films. Tartu, 2011.
79. **Сергей Наконечный.** Исследование электронно-дырочных и интерстициал-вакансионных процессов в монокристаллах MgO и LiF методами термоактивационной спектроскопии. Тарту, 2011.
80. **Niina Voropajeva.** Elementary excitations near the boundary of a strongly correlated crystal. Tartu, 2011.
81. **Martin Timusk.** Development and characterization of hybrid electro-optical materials. Tartu, 2012, 106 p.
82. **Merle Lust.** Assessment of dose components to Estonian population. Tartu, 2012, 84 p.